Phase diagram of the charged black hole bomb system

Alex Davey, Oscar J. C. Dias, and Paul Rodgers

STAG research centre and Mathematical Sciences, University of Southampton,
Southampton SO17 1BJ, U.K.

E-mail: amd1g13@soton.ac.uk, ojcd1r13@soton.ac.uk, pwr1u17@soton.ac.uk

ABSTRACT: We find the phase diagram of solutions of the charged black hole bomb system. In particular, we find the static hairy black holes of Einstein-Maxwell-Scalar theory confined in a Minkowski box. We impose boundary conditions such that the scalar field vanishes at and outside a cavity of constant radius. These hairy black holes are asymptotically flat with a scalar condensate floating above the horizon. We identify four critical scalar charges which mark significant changes in the qualitative features of the phase diagram. When they coexist, hairy black holes always have higher entropy than the Reissner-Nordström black hole with the same quasilocal mass and charge. So hairy black holes are natural candidates for the endpoint of the superradiant/near-horizon instabilities of the black hole bomb system. We also relate hairy black holes to the boson stars of the theory. When it has a zero horizon radius limit, the hairy black hole family terminates on the boson star family. Finally, we find the Israel surface tensor of the box required to confine the scalar condensate and that it can obey suitable energy conditions.

Contents

1 Introduction

The black hole bomb setup was designed by Zel'dovich [1] and Press and Teukolsky [2] (see also [3]) very much in the aftermath of having understood the mathematical theory of black hole perturbations around a Kerr black hole. It emerged naturally from the fact that the wave analogue of the Penrose-Christodoulou process [4, 5] — superradiant scattering — unavoidably occurs in rotating black holes with angular velocity Ω. If a scalar wave with frequency ω and azimuthal number m satisfying $\omega < m\Omega$ is trapped near the horizon by the potential of a box (for example), the multiple superradiant amplifications and reflections at the cavity lead to an instability. The wave keeps extracting energy and angular momentum from the black hole interior and these accumulate between the horizon and the cavity. Press and Teukolsky assumed that this build up of radiation pressure would raise to levels that could no longer be supported by the box and the latter would eventually break apart. But the black hole bomb system does not necessarily need to have such a dreadful end. Actually, more often than not, a black hole instability is a pathway to find new solutions that are stable to the original instability, have more entropy (for given energy and angular momentum) and are thus natural candidates for the endpoint or metastable states of the instability time evolution. This is certainly the case for superradiant fields trapped by the anti-de Sitter (AdS) gravitational potential [6–11] or massive fields in asymptotically flat black holes [12]. So we can expect the same in the original black hole bomb system.

Motivated by these considerations, we would like to find the full phase diagram of solutions that can exist in the original black hole (BH) bomb system. By this we mean to

find all possible stationary solutions of the theory with boundary conditions that confine the scalar field inside the box. These would be the non-linear version of the floating solutions in equilibrium that are described in [2]. This certainly requires solving PDEs. Therefore, in this paper, we start by considering a simpler system that still has a superradiant scalar field trapped inside a box but those properties can be found solving simply ODEs. This is possible if we first place a Reissner-Nordström black hole (RN BH) with chemical potential μ inside a box and then perturb it with a scalar field with charge q and frequency ω. As long as $\omega < q\mu$, a superradiant instability will also develop leading to the charged version of the black hole bomb system [13]. We thus want to find the phase diagram of static solutions of this system, including those with a scalar condensate floating above the horizon. The latter hairy solutions might have higher entropy than the original RN BH for a given energy and charge where they coexist. If so they would be a natural candidate for the endpoint of the charged black hole bomb instability, as long as we check that we can build boxes — with an Israel stress tensor [14–17] that satisfies the relevant energy conditions [18] — that holds the internal radiation pressure without breaking apart. This will further guarantee that we can insert this boxed system in an exterior Reissner-Nordström background, as required by Birkhoff's theorem [19, 20].

Looking into the details of this programme we immediately find new physics. Indeed, a linear perturbation analysis of the Klein-Gordon equation in an RN BH finds that the system is not only unstable to superradiance but also to the near-horizon scalar condensation instability [21]. These two instabilities are typically entangled for generic RN BHs but there are two corners of the phase space where they disentangle and reveal their origin. Indeed, extremal RN BHs with arbitrarily small horizon radius only have the superradiant instability since the near-horizon instability is suppressed as inverse powers of the horizon radius. On the opposite corner, RN BHs with a horizon radius close to the box radius only have the near horizon instability. Essentially, this instability is triggered by scalar fields that violate the near horizon AdS_2 Breitenlöhner-Freedman (BF) bound [22] of the extremal RN BH. It was originally found by Gubser [23] in planar AdS backgrounds (in a study that initiated the superconductor holographic programme) but it exists in other BH backgrounds (independently of the cosmological constant sign) with an extremal (zero temperature) configuration (see *e.g.* [24, 25]).

Analysing the setup of the black hole bomb system leads to the observation that the theory also has horizonless solutions if we remove the RN BH but leave the scalar field inside a box with a Maxwell field. Indeed, we can certainly perturb a Klein-Gordon field in a cavity and the frequencies that can fit inside it will be naturally quantized and real. This suggests that, within perturbation theory, we can then back-react this linear solution to higher orders where it will source non-trivial gravitoelectric fields that are regular inside (and outside) the box [26]. These are the boson stars of the theory, also known as solitons (depending on the chosen U(1) gauge; see *e.g.* [27] for a review on boson stars). This perturbative analysis is bound to capture only small mass/charge boson stars. But a full numerical nonlinear analysis can identify the whole phase space of boson stars [28]. This analysis further reveals that the phase diagram of boson stars is quite elaborate with distinct boson star families. In particular, it finds that the phase diagram of solitons

depends non-trivially on a total of four critical scalar field charges. Two of them can be anticipated using simple heuristic arguments on the aforementioned superradiant and near-horizon instabilities, but the two others only emerge after solving the non-linear equations of motion.

Coming back to our main subject of study, an RN BH placed inside a box is also the starting point to discuss and find the hairy BHs of the theory. The latter have a scalar condensate floating above the horizon that is balanced against gravitational collapse by electric repulsion. A box with appropriate Israel junction conditions and stress tensor [14–17] should be able to confine the scalar condensate in its interior, and it should then be possible to place the whole boxed system in a background whose exterior solution is the RN solution. In the present paper, we confirm that this is indeed the case and we find the full phase diagram of static solutions of the charged black hole bomb system. It turns out that the aforementioned four critical scalar electric charges play a relevant role also in the phase diagram of hairy BHs. Indeed, this diagram is qualitatively distinct depending on which one of the four available windows of critical charges the scalar charge q falls into. Ultimately, the reason for this dependence follows from the fact — that we will establish — that all hairy BHs that have a zero horizon radius limit choose to terminate on the boson star of the theory (which is fully specified once q is given), in the sense that the zero entropy hairy BHs have the same (Brown-York [29] quasilocal) mass and charge as the boson star. In our system, this materializes the idea that, often, small hairy BHs can be thought of as a small BH (RN or Kerr BH) placed on top of a boson star, as long as they have the same thermodynamic potential (chemical potential or angular velocity) to have the two constituents in thermodynamic equilibrium.

One of the four hairy BH families that we find in this paper was already identified in the perturbative analysis of [26]. This is the only family of hairy BHs that extends to arbitrarily small mass and charge, thus making it prone to be captured by the perturbative analysis about an empty box with an electric field. But the other three families and their intricate properties cannot be captured by such a theory because they are not perturbatively connected to the zero mass/charge solution.

Perhaps the most important property of the hairy BHs of the charged black hole bomb is that, when both coexist, they *always* have higher entropy than the RN BH that has the *same* mass and charge. Therefore, we will conclude that hairy BHs are always the preferred thermodynamic phase of the theory in the microcanonical ensemble.

Very much like black holes confined in a box can be the a starting point to discuss certain aspects of black hole thermodynamics [30–36] they should also be useful to understand generic superradiant systems where distinct (including perhaps some astrophysical) potential barriers confine fields [2]. These two are related since the hairy solutions describe non-linear systems where the central solution is in thermodynamic equilibrium with the floating scalar radiation. In particular, we can expect that hairy solutions of the charged black hole bomb provide a toy model with *some* universal features for the phase diagram of other confined unstable systems. Actually, we find that the present phase diagram shares many common features with the phase diagram of superradiant hairy blacks holes in global anti-de Sitter [25, 37–43].

The plan of our manuscript is as follows. In section 2 we summarize in two figures the main properties of the phase diagram of hairy black holes and boson stars. In section 3 we formulate the exact setup of our system. The discussion only includes aspects that guarantee that our exposition is self-contained and more details can be found in [26]. In section 4 we explicitly construct the hairy black hole solutions in the four relevant windows of scalar charge that, together with the boson star study of [28], allow us to arrive to the conclusions summarized in section 2. Finally, in section 5 we explain how data of the hairy solution inside the box can be used to find the Israel stress tensor of the cavity surface layer and be matched with the exterior Reissner-Nordstöm solution.

2 Summary of phase diagram of boson stars and black holes in a cavity

The Einstein-Maxwell-Klein-Gordon theory, whereby the scalar field is confined inside a box of radius L in an asymptotically flat background, is fully specified once we fix the mass and charge q of the scalar field. We consider massless scalar fields with dimensionless electric charge $e = qL$ (the system has a scaling symmetry that allows us to measure all physical, *i.e.* dimensionless, quantities in units of L). By Birkhoff's theorem [19, 20],[1] outside the cavity the hairy solutions we search for are necessarily described by the RN solution. Thus, we just need to find the hairy solutions inside the box and then confirm that the Israel junctions conditions required to confine the scalar condensate inside the cavity, while having an exterior RN solution, correspond to an Israel energy-momentum stress tensor (proportional to the extrinsic curvature jump across the box layer [14–17]) that is physical, *i.e.* that satisfies relevant energy conditions [18].

Since the solution outside the box is described by the RN solution, we cannot use the Arnowitt-Deser-Misner (ADM) mass M and charge Q [44] to differentiate the several solutions of the theory. However, we can use the Brown-York quasilocal mass $\mathcal{M}$ and charge $\mathcal{Q}$ [29], computed at the box location and normalized in units of L, and associated phase diagram $\mathcal{Q}$-$\mathcal{M}$ to display and distinguish the solutions of the theory. These quasilocal quantities obey their own first law of thermodynamics that is used to (further) check the results. In the quasilocal phase diagram, the extremal RN 1-parameter family of BHs (with horizon inside the box) provides a natural reference to frame our discussions. In particular, because distinct solutions often pile-up in certain regions of the phase diagram, for clarity we will find it useful to plot $\Delta\mathcal{M}/L$ *vs* $\mathcal{Q}/L$ where $\Delta\mathcal{M} = \mathcal{M} - \mathcal{M}\big|_{\mathrm{ext\,RN}}$ is the mass difference between the hairy solution and the extremal RN that has the *same* $\mathcal{Q}/L$. Therefore, in this phase diagram $\mathcal{Q}$-$\Delta\mathcal{M}$, the horizontal line with $\Delta\mathcal{M} = 0$ represents the extremal RN BH solution. Its horizon at R_+ fits inside the box of radius L if $R_+ \leq 1$ (which corresponds to $\mathcal{Q}/L \leq 2^{-1/2}$) and non-extremal RN BHs exist above this line. However, horizons of non-extremal RN BHs fit inside the box ($R_+ \leq 1$) if and only if their quasilocal charges are to the left of the red dashed line that we will display in our $\mathcal{Q}$-$\Delta\mathcal{M}$ diagrams.

---

[1]Birkhoff's theorem for Einstein-Maxwell theory states that the unique spherically symmetric solution of the Einstein-Maxwell equations with non-constant area radius function r (in the gauge (3.2)) is the Reissner-Nordström solution. If r is constant then the theorem does not apply since one has the Bertotti-Robinson ($AdS_2 \times S^2$) solution.

Actually, it turns out that this line also represents the maximal quasilocal charge that hairy solutions enclosed in the box can have.

We find that the spectrum of hairy black holes and boson stars of the theory is qualitatively distinct depending on whether e is smaller or bigger than four pivotal critical scalar field charges — e_{NH}, e_γ, e_c and e_{S} — which obey the relations $0 < e_{\mathrm{NH}} < e_\gamma < e_c < e_{\mathrm{S}}$.

Two of these critical charges, e_{NH} and e_{S}, can be identified simply studying linear scalar field perturbations about an RN BH in a box. Such RN BHs can be parametrized by the chemical potential μ and dimensionless horizon radius $R_+ = r_+/L$. These parameters are constrained to the intervals $0 \leq \mu \leq \mu_{\mathrm{ext}}$ (with the upper bound being the extremal configuration) and $0 < R_+ \leq 1$. Boxed RN BHs become unstable — the black hole bomb system — if e is above the instability onset charge $e_{\mathrm{onset}}(\mu, R_+)$. Instead of displaying $e_{\mathrm{onset}}(\mu, R_+)$, it proves to be more clear to display the 2-dimensional plot $e_{\mathrm{onset}}(R_+)$ for fixed values of μ. A sketch of this plot is given in the left panel of figure 1 (which reproduces the exact results in figure 2 of [21]). The minimal onset charge is attained for extremal RN black holes ($\mu = \mu_{\mathrm{ext}}$): this is the orange curve that connects points $(0, e_{\mathrm{S}})$ and $(1, e_{\mathrm{NH}})$. For completeness, in the left panel of figure 1 we also sketch the onset charge curves (green dashed) for two non-extremal RN BHs at fixed $\mu < \mu_{\mathrm{ext}}$. Naturally, this onset charge increases as we move away from extremality. Moreover, we see that the (extremal) minimal onset curve terminates at two critical charges that, actually, can be computed analytically:

- $e = e_{\mathrm{NH}} = \frac{1}{2\sqrt{2}} \sim 0.354$. This is the charge above which scalar fields can trigger a violation of the near horizon AdS_2 Breitenlöhner-Freedman (BF) bound [22–25] of the extremal RN black hole whose horizon radius approaches, from below, the box radius. For details on how to derive this critical charge please refer to section III.B of [21].

- $e = e_{\mathrm{S}} = \frac{\pi}{\sqrt{2}} \sim 2.221$. This is the critical charge above which scalar fields can drive arbitrarily small RN BHs unstable via superradiance. For a detailed analysis that leads to this critical charge, please see section III.A of [26].

The system has two other critical charges, e_γ and e_c, that are uncovered when we do a detailed scan of the boson stars (a.k.a. solitons) of the theory. This task was completed in detail in the companion paper [28]. A phase diagram that summarizes the relevant properties for the present study is displayed in the right panel of figure 1 [28]. Note that it stores in a single plot the solitons for *different theories*, *i.e.* for several distinct values of e. Two families of ground state boson stars (*i.e.* with smallest energy for a given charge) where found in [28]. One is the *main or perturbative boson star family* which can be found within perturbation theory if we back-react a normal mode of a Minkowski cavity to higher orders. In the right panel of figure 1, these are the solitons that are continuously connected to $(\mathcal{Q}, \Delta\mathcal{M}) = (0, 0)$. The other one is the *secondary or non-perturbative soliton family*. In figure 1, these are the solitons that exist only above a critical $\mathcal{Q}$ and terminate at the red dashed line. The main/perturbative soliton family exists for any value of $e > 0$ (the system has a symmetry that allows us to consider only
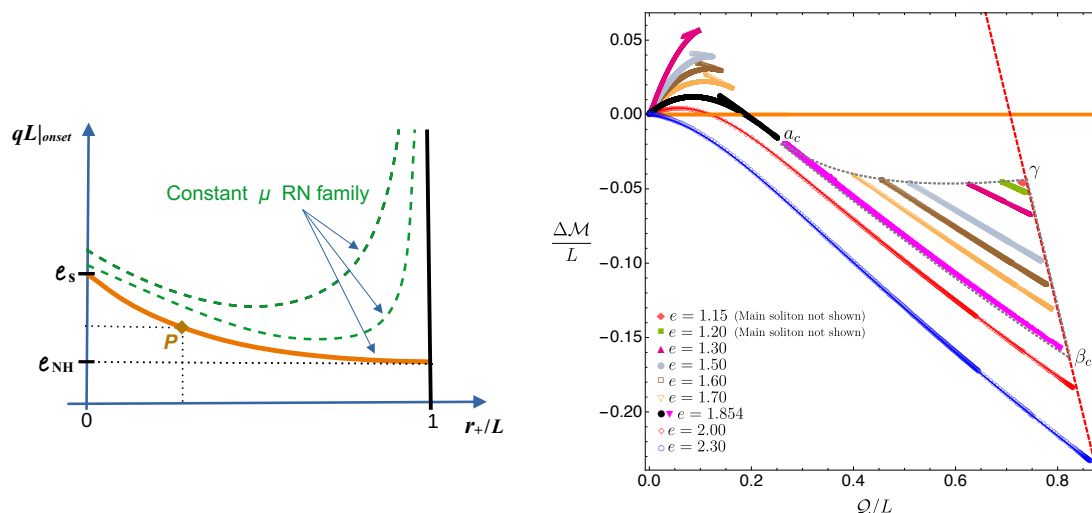
Figure 1. *Left panel:* sketch of the scalar field electric charge $e_{\rm onset} = qL|_{\rm onset}$ as a function of the horizon radius $R_+ = r_+/L$ of RN BHs in a box (sketched from figure 2 of [21]). The orange curve in the bottom — that starts at $(R_+, e) = (0, e_{\rm S})$ and terminates at $(R_+, e) = (1, e_{\rm NH})$ — describes the *minimal* onset charge (which occurs at extremality, $\mu = \mu_{\rm ext}$). That is, (non-)extremal RN BHs can be unstable if an only if e is higher than the one identified by this orange onset curve. On the other hand, if we pick an RN family with constant $\mu < \mu_{\rm ext}$, for instability, we need e to be higher than the associated green dashed line $e(R_+)|_{\rm const\,\mu}$ also shown. In particular, we see that if we chose a charge in the range $e_{\rm NH} \leq e \leq e_{\rm S}$, RN BHs are unstable if and only if they are between the orange minimal onset curve and the horizontal line to the right of point P (gold diamond). *Right panel:* a survey of boson stars for different values of e, for $e \geq e_\gamma$ [28]. For a given $e \in [e_\gamma, e_c[$ we have the main (perturbatively connected to $(0,0)$) and secondary (non-pertubative) solitons (which only exist in the region bounded by the auxiliary grey dashed closed curve $a_c \beta_c \gamma$). The secondary soliton curve with e just above e_γ is close to the point γ, while the soliton with $e = 1.854$, just below e_c, is the magenta curve (very close to $a_c \beta_c$). Note that the gap in $\mathcal{Q}/L$ between the main soliton and the secondary one starts very large at $e = e_\gamma$ but then decreases and goes to zero precisely at $e = e_c$.

$e > 0$). However, the secondary/non-perturbative soliton only exists for scalar field charges that are in the window $e_\gamma \leq e < e_c$. These are the solitons enclosed in the region $a_c \beta_c \gamma$ (*i.e.* inside the auxiliary grey dashed closed line with these vertices). They only exist above $e_\gamma \sim 1.13$ (see point γ) and below $e_c \simeq 1.854 \pm 0.0005$ (see line $a_c \beta_c$ just below the magenta line). Below e_γ the non-perturbative solitons do not exist because they no longer fit inside the box. Above e_c, the gap between the two soliton families ceases to exist, *i.e.* the non-perturbative soliton merges with the perturbative soliton, and the ground state boson stars of the theory extend from the origin all the away to the red dashed line (see *e.g.* the red diamond curve with $e = 2$ or the blue circle curve with $e = 2.3$ in figure 1). Summarizing, the main/perturbative soliton has a Chandrasekhar limit for $0 < e < e_c$ but extends from the origin all the way to the red dashed line for $e \geq e_c$. On the other hand, the ground state secondary/non-perturbative soliton only exists in the window $e_\gamma \leq e < e_c$.

In the following sections we will find the hairy black holes of the Einstein-Maxwell-Klein-Gordon theory. We will conclude that, whenever the hairy black holes have a zero
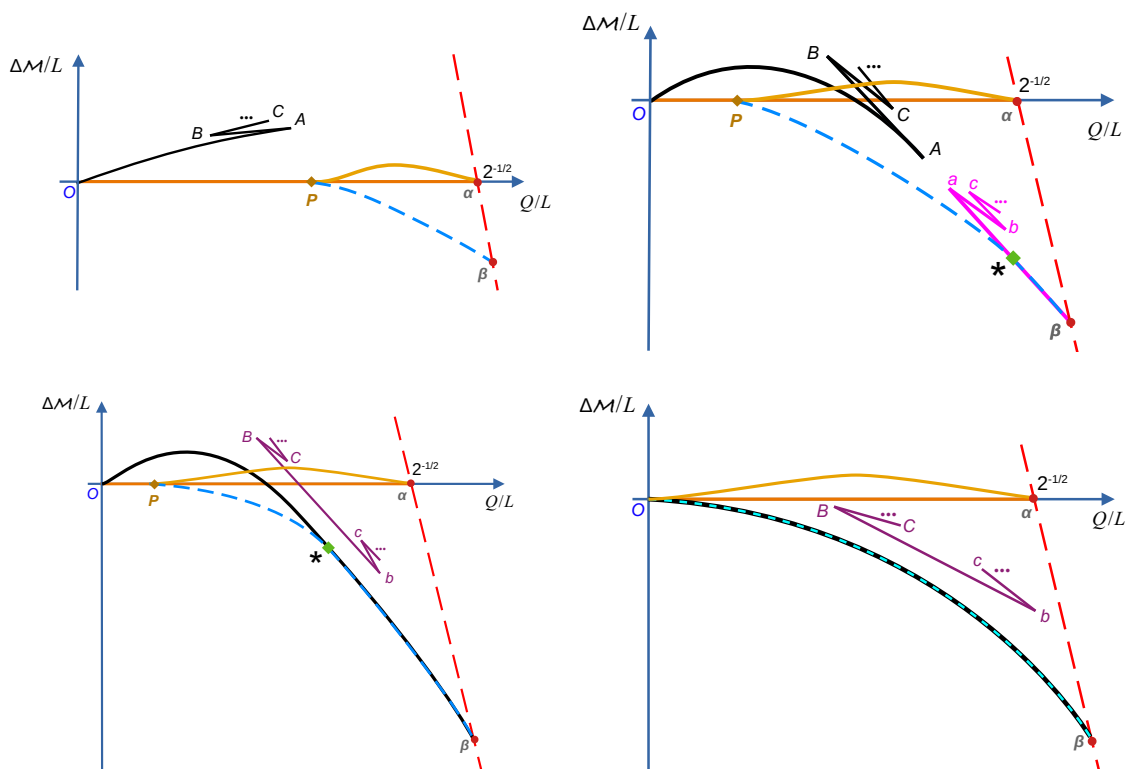
Figure 2. Sketch of the quasilocal phase diagram for black holes and solitons and as we span relevant windows of scalar field charge e. The critical charges are such that $0 < e_{\mathrm{NH}} < e_\gamma < e_c < e_{\mathrm{S}}$. The quantity $\Delta\mathcal{M}$ is the quasilocal mass difference between a given solution and an extremal RN BH that has the *same* quasilocal charge $\mathcal{Q}/L$. Hence the orange line at $\Delta\mathcal{M} = 0$ describes the extremal RN solution that must have $\mathcal{Q}/L \leq 2^{-1/2}$ to fit inside the box. The red dashed line represents the maximal quasilocal charge of solutions that can fit inside the box. It intersects the extremal RN line at $\mathcal{Q}/L = 2^{-1/2}$. Non-extremal RN BHs confined in the box have $\Delta\mathcal{M} > 0$ and fill the triangular region bounded by $\mathcal{Q} = 0$ and by the orange and red dashed lines (not shown completely). The main soliton family is always given by black curves that start at O. The secondary soliton family is given either by magenta or purple curves. Hairy black holes exist in the region $P\alpha\beta$ enclosed by the yellow merger line $P\alpha$ (between hairy and RN BHs), the blue curve $P\beta$ where the curvature grows large and the red line $\alpha\beta$. *Top-left panel:* case $e_{\mathrm{NH}} < e < e_\gamma$. *Top-right panel:* $e_\gamma \leq e < e_c$. *Bottom-left panel:* case $e_c \leq e < e_{\mathrm{S}}$. *Bottom-right panel:* case $e \geq e_{\mathrm{S}}$.

horizon radius limit, they terminate on a soliton. Accordingly, the phase diagram of solutions depends on the above four critical scalar field charges. Our main findings are summarized in the phase diagram sketches of figure 2 and the properties of these phase diagrams depend on the following 5 windows of scalar charge e:

1. $e < e_{\mathrm{NH}} = \frac{1}{2\sqrt{2}} \sim 0.354$. From the left panel of figure 1, one concludes that RN is stable for $e < e_{\mathrm{NH}}$ and thus no hairy BHs exist. The only non-trivial solutions of the theory are the RN BH and the main/perturbative boson star which has a Chandrasekhar limit (see details in [28]).

2. $e_{\mathrm{NH}} \leq e < e_\gamma \sim 1.13$. The phase diagram $\mathcal{Q}$-$\Delta\mathcal{M}$ of solutions for this window is sketched in the top-left panel of figure 2. The only boson star of the theory is the main/perturbative family $OABC\cdots$ (already present for $e < e_{\mathrm{NH}}$) with its Chandrasekhar limit A and a series of cusps $A, B, C, \cdots$ and associated zig-zagged branches whose properties were studied in detail in [28]. As the left panel of figure 1 indicates, RN BHs are now unstable for sufficiently large R_+ (*i.e.* $\mathcal{Q}$) if sufficiently close to extremality (see diamond point P and region bounded by the horizontal line to the right of P and the minimal onset curve). The onset of the instability translates into the yellow curve $P\alpha$ in the top-left panel of figure 2 and RN BHs below this onset curve $P\alpha$ (and above the extremal horizontal straight line $OP\alpha$) are unstable. Hairy BHs exist inside the region bounded by the closed curve $P\alpha\beta$. They merge with RN BHs at the onset $P\alpha$ of the instability and they extend for lower masses all the way down to the blue dashed line $P\beta$ where they terminate at *finite* entropy and *zero* temperature because the Kretschmann curvature at the horizon blows up. They are also constrained to be to the left of the red dashed line $\alpha\beta$ because the horizon of the hairy BH must fit inside the cavity with unit normalized radius. Note that for this window of e there is no dialogue between the hairy boson star and the hairy BH families.

   A representative example of a black hole bomb system with a charge $e = 1$ in this window $e_{\mathrm{NH}} \leq e < e_\gamma$ will be discussed in detail in section 4.1 and figure 3.

3. $e_\gamma \leq e < e_c \simeq 1.854 \pm 0.0005$. The phase diagram $\mathcal{Q}$-$\Delta\mathcal{M}$ of solutions for this window is sketched in the top-right panel of figure 2. Besides the main/perturbative family $OABC\cdots$ of boson stars (black line), the system now has the secondary/non-perturbative family $\beta abc\cdots$ of boson stars (magenta line) and there is a gap Aa between these two families. Precisely at e_γ, this gap Aa is the largest and the non-perturbative boson star family reduces to a single point β on top of the red-dashed line (*i.e.* it coincides with point γ in right panel of figure 1). As e grows beyond e_γ, the gap Aa decreases and it vanishes precisely at $e = e_c$ where the two ground state soliton families merge into a single one (for details of this merger please see [28]).

   As before, hairy BHs exist in the region enclosed by the closed line $P\alpha\beta$ with the yellow curve $P\alpha$ being again the instability onset curve where the scalar condensate vanishes and hairy BHs merge with the RN BH family. As before, the hairy BHs also extend for smaller masses all the way down to the singular blue dashed line $P\beta$ where the Kretschmann curvature at the horizon diverges. But this time, this singular curve $P\beta \equiv P\star\beta$ splits into two segments. Hairy BHs terminating in the trench $P\star$ do so at *finite entropy* and *zero temperature*, as all the hairy BHs with $e < e_c$. However, hairy BHs terminating at the trench $\star\beta$ do so at *zero entropy* and *infinite temperature*. In such a way that in the $\mathcal{Q}$-$\Delta\mathcal{M}$ phase diagram, this hairy BH trench $\star\beta$ *coincides* with the secondary/non-perturbative soliton (magenta line between $\star$ and β). In this sense, we can say that hairy BHs with large charge ($\mathcal{Q} \geq \mathcal{Q}_\star$) terminate on the non-perturbative soliton. This point $\star$ coincides with β in the limit $e \to e_\gamma$ and it diverges away from β as e moves away from e_γ towards e_c.

A representative example of a black hole bomb system with a charge $e = 1.85$ in this window $e_\gamma \leq e < e_c$ will be discussed in detail in section 4.2 and figures 4–6.

4. $e_c \leq e < e_{\rm S} = \frac{\pi}{\sqrt{2}} \sim 2.221$. The phase diagram $\mathcal{Q}$-$\Delta\mathcal{M}$ of solutions for this window is sketched in the bottom-left panel of figure 2. At $e = e_c$ the perturbative and non-perturbative boson star families merge and for $e \geq e_c$ the boson star ground state is always the perturbative family $O\beta$ (black curve) that extends from the origin to the red dashed line. There is also a secondary family of boson stars $\cdots CBbc \cdots$ (purple curve) but it is not the ground state family and it plays no role in the description of hairy BHs. Therefore we do not discuss it further (see [28] for details).

Hairy BHs exist inside the closed line $P\alpha\beta$. Again, the yellow curve $P\alpha$ is the instability onset curve where hairy BHs merge with the RN BH family. The hairy BHs extend for smaller masses all the way down to the singular blue dashed line $P\star\beta$ where the Kretschmann curvature at the horizon diverges. Hairy BHs terminating in the trench $P\star$ do so at *finite entropy* and *zero temperature*, while hairy BHs terminating at the trench $\star\beta$ do so at *zero entropy* and *infinite temperature*. In the $\mathcal{Q}$-$\Delta\mathcal{M}$ phase diagram, this hairy BH trench $\star\beta$ *coincides* with the perturbative soliton (black line between $\star$ and β). In this sense, hairy BHs with large charge ($\mathcal{Q} \geq \mathcal{Q}_\star$) terminate on the perturbative soliton. As e increases above e_c, points P and $\star$ move to the left of the phase diagram, *i.e.* to lower values of $\mathcal{Q}$ and they approach the origin O as $e \to e_{\rm S}$.

A representative example of a black hole bomb system with a charge $e = 2$ in this window $e_c \leq e < e_{\rm S}$ will be discussed in detail in section 4.3 and figures 7–9.

5. $e \geq e_{\rm S}$. The phase diagram $\mathcal{Q}$-$\Delta\mathcal{M}$ of solutions for this window is sketched in the bottom-right panel of figure 2. Precisely at $e_{\rm S}$, the slope $\mathrm{d}\Delta\mathcal{M}/\mathrm{d}\mathcal{Q}$ of the main/ perturbative boson star family (black curve $O\beta$) vanishes at the origin and for $e \geq e_{\rm S}$, perturbative boson stars always have $\Delta\mathcal{M} < 0$. Not less importantly, at and above $e_{\rm S}$, all extremal RN BHs are unstable, *i.e.* point P seen in the plots for $e < e_{\rm S}$ hits the origin O. Consequently, hairy BHs now exist for all values of $\mathcal{Q}$ (that can fit inside the cavity), *i.e.* in the 2-dimensional region with boundary $O\alpha\beta$. And, for any $\mathcal{Q}$, hairy BHs bifurcate from RN at the instability onset $O\alpha$ (yellow curve) and extend for smaller masses till they terminate − with zero entropy, and divergent temperature and Kretschmann curvature − along a curve (blue dashed line) that *coincides* with the boson star curve $O\beta$ (black curve).

A representative example of a black hole bomb system with a charge $e = 2.3$ in this window $e \geq e_{\rm S}$ will be discussed in detail in section 4.4 and figures 10–12.

Independently of e, a universal property of hairy BHs is that, when they coexist with boxed RN BHs, they always have higher entropy than the boxed RN BH with the same quasilocal mass and charge. That is to say, in the phase space region where they exist, hairy BHs are always the dominant phase in microcanonical ensemble. Moreover, hairy BHs are stable to the superradiant mode that drives the boxed RN BH unstable. It follows from these observations and the second law of thermodynamics that the endpoint of the superradiant/near horizon instability of the boxed RN BH, when we do a time evolution

at constant mass and charge, should be a hairy BH. It would be interesting to confirm this doing time evolutions along the lines of those done in [45–47].

The present work can be seen as the final study of a sequel of works on the charged black hole bomb system. Ref. [21] started by studying the linear superradiant and near-horizon instabilities of the boxed RN BH. This identified the zero-mode and growth rates of these instabilities. The hairy boson stars and hairy BHs were found within perturbation theory in [26]. As expected, this perturbative analysis is valid only for small condensate amplitudes and small horizon radius and thus it is able to capture only small energy/charge hairy solutions. Therefore, for the solitons, the perturbative analysis can capture the main or perturbative boson star family at small mass/charge. But it misses: 1) the existence of the Chandrasekhar limit and cusps of this family, 2) the existence of the secondary or non-perturbative boson star family, and 3) it misses the existence of two important critical charges e_γ and e_c where the non-perturbative soliton starts existing and merges with the perturbative family. These properties were only identified once the Einstein-Maxwell-Klein-Gordon equation was solved fully non-linearly in [28]. On the other hand, the perturbative analysis of [26] also finds the hairy BHs that, for $e \geq e_{\rm s}$, are perturbatively connected to a Minkowski spacetime with a cavity. By construction, these perturbative hairy BHs reduce, in the zero horizon radius limit, to the boson star of the theory. However, the perturbative analysis of [26] says nothing about the hairy BHs of the theory when $e < e_{\rm s}$. In the present manuscript, we fill this gap.

In the introduction we already mentioned that the potential barrier that confines the scalar condensate in our boxed or black hole bomb system might be a good toy model for other systems with potential barriers that provide confinement. In particular, we find that the phase diagram of hairy boson stars and BHs in the black hole bomb system is qualitatively similar to the one found for asymptotically anti-de Sitter solitons [25, 37–43]. In this latter case, the AdS boundary conditions act as a natural gravitational box with radius inversely proportional to the cosmological length that provides bound states. In this sense, our work also complements and completes previous AdS studies since the existence range of the secondary/non-perturbative boson star family, its merger with the main/perturbative soliton at $e = e_c$, and the fact that hairy BHs can also terminate on this soliton family for $e_\gamma \leq e < e_c$ was not established in detail in [25, 37–40].

3 Setting up the black hole bomb boundary value problem

The setup of our problem was already discussed in the perturbative analysis of the problem in [26]. Here, to have a self-contained exposition, we discuss only the key aspects needed to formulate the problem and the strategy to compute physical quantities without ambiguities. We ask the reader to see [26] for details.

3.1 Einstein-Maxwell gravity with a confined scalar field

We consider the action for Einstein-Maxwell-Klein-Gordon gravity:

$$S = \frac{1}{16\pi G_N} \int {\rm d}^4 x \sqrt{g} \left(\mathcal{R} - \frac{1}{2} F_{\mu\nu} F^{\mu\nu} - 2 D_\mu \phi (D^\mu \phi)^\dagger + m^2 \phi \phi^\dagger \right), \qquad (3.1)$$

where $\mathcal{R}$ is the Ricci scalar, A is the Maxwell gauge potential, $F = \mathrm{d}A$, $D_\mu = \nabla_\mu - iqA_\mu$ is the gauge covariant derivative of the system, and ϕ is a complex scalar field with mass m and charge q. We consider only massless scalar fields, although it is certainly possible to extend our analysis to $m > 0$. We fix Newton's constant $G_N \equiv 1$.

We want to find the black hole solutions of (3.1) that are static, spherically symmetric and asymptotically flat. U(1) gauge transformations allow us to work with a real scalar field and a gauge potential that vanishes at the horizon. Further choosing the Schwarzschild gauge, an *ansatz* with the desired symmetries is then

$$\mathrm{d}s^2 = -f(r)\mathrm{d}t^2 + g(r)\mathrm{d}r^2 + r^2\mathrm{d}\Omega_2^2, \qquad A_\mu\mathrm{d}x^\mu = A(r)\mathrm{d}t, \qquad \phi = \phi^\dagger = \phi(r), \quad (3.2)$$

with $\mathrm{d}\Omega_2^2$ being the metric for the unit 2-sphere (expressed in terms of the polar and azimuthal angles $x = \cos\theta$ and φ). The scalar field is forced to be confined inside a box of radius L. The system then has a scaling symmetry that allows us to normalize coordinates $(T = t/L, R = r/L)$ and thermodynamic quantities in units of L, and place the box at radius $R = 1$ [26].

In these conditions, the equations of motion that follow from (3.1) can be found in [26]. These are a set of three ordinary differential equations for the fields $f(R)$, $A(R)$ and $\phi(R)$, and an algebraic equation that expresses $g(R)$ as a function of the other 3 fields and their first derivatives. Well-posedness of the boundary value problem requires that we give boundary conditions at the horizon and asymptotic boundary of our spacetime. Additionally, we must specify Israel junction conditions at the timelike hypersurface $\Sigma = R - 1 = 0$ where the box is located. Again, our hairy BHs have vanishing scalar field at and outside this box, $\phi(R \geq 1) = 0$.

The horizon, with radius $R = R_+ = \frac{r_+}{L}$ is the locus $f(R_+) = 0$. We have three second order ODEs and thus there are six free parameters when we do a Taylor expansion about the horizon. Regularity demands Dirichlet boundary conditions that set three of these parameters to zero. We are thus left with only three constants f_0, A_0, ϕ_0 (say) such that the regular fields have the Taylor expansion around the origin:

$$\begin{aligned} f(R_+) &= f_0(R - R_+) + \mathcal{O}((R - R_+)^2), \\ A(R_+) &= A_0(R - R_+) + \mathcal{O}((R - R_+)^2), \qquad \phi(R_+) = \phi_0 + \mathcal{O}((R - R_+)^2). \end{aligned} \quad (3.3)$$

Consider now the asymptotic boundary of our spacetime, $R \to \infty$. The scalar field vanishes outside the box, $\phi = 0$, and the equations of motion have the solution: $f^{\mathrm{out}}(R) = c_f - \frac{M_0}{R} + \frac{\rho^2}{2R^2}$, $A_t^{\mathrm{out}}(R) = c_A + \frac{\rho}{R}$ and $g^{\mathrm{out}}(R) = c_f/f^{\mathrm{out}}(R)$ (onwards, the superscript $^{\mathrm{out}}$ represents fields outside the cavity). Here, c_f, M_0, c_A and ρ are arbitrary parameters, *i.e.* we have an asymptotically flat solution for any value of these constants. However, the theory has a second scaling symmetry $(e = qL)$

$$\{T, R, x, \varphi\} \to \{\lambda_2 T, R, x, \varphi\}, \quad \{f, g, A_t, \varphi\} \to \{\lambda_2^{-2}f, g, \lambda_2^{-1}A_t, \varphi\}, \quad \{e, R_+\} \to \{e, R_+\}, \quad (3.4)$$

that we use to set $c_f = 1$ so that $f|_{r\to\infty} = 1$ (and $g^{\mathrm{out}} = 1/f^{\mathrm{out}}$) [26]. Outside the box the solution to the equations of motion is then

$$f^{\mathrm{out}}(R)|_{R\geq 1} = 1 - \frac{M_0}{R} + \frac{\rho^2}{2R^2}, \qquad A_t^{\mathrm{out}}(R)|_{R\geq 1} = c_A + \frac{\rho}{R}, \qquad \phi^{\mathrm{out}}(R)|_{R\geq 1} = 0. \quad (3.5)$$

As required by Birkhoff's theorem for the Einstein-Maxwell theory [19, 20], this is the Reissner-Nordström (RN) solution. The leftover free constants in (3.5), M_0, c_A, ρ, will be determined only after we have the solution inside the cavity and specify the Israel junctions conditions at the latter.

Some of the parameters in (3.5) are related to the ADM conserved charges [44]. Indeed, the dimensionless ADM mass and electric charge of the system are $(G_N \equiv 1)$:[2]

$$M/L = \lim_{R\to\infty} \frac{R^2 f'(R)}{2\sqrt{f(R)g(R)}} = \frac{M_0}{2}, \qquad Q/L = \lim_{R\to\infty} \frac{R^2 A_t'(R)}{2f(R)g(R)} = -\frac{\rho}{2}. \qquad (3.6)$$

These ADM conserved charges measured at the asymptotic boundary include the contribution from the energy-momentum content of the cavity that confines the scalar hair. In the next subsection we discuss the properties of this box.

In these conditions, hairy BHs of the theory are a 2-parameter family of solutions that we can take to be the horizon radius R_+ and the value of the (interior) derivative of the scalar field at the box, $\epsilon \equiv \phi'^{\,in}|_{R=1^-}$.

As mentioned in section 2, it follows from Birkhoff's theorem that in the asymptotic region our solutions are necessarily described by the RN solution. Therefore, the ADM mass M and charge Q cannot be used to distinguish the several solutions of the theory. It is thus natural to instead use the Brown-York quasilocal mass $\mathcal{M}$ and charge $\mathcal{Q}$, measured at the box, to display our solutions in a phase diagram of the theory [29]. From section II.C of [26], the Brown-York quasilocal mass and charge contained inside a 2-sphere with radius $R = 1$ are $(G_N \equiv 1)$[3]

$$\mathcal{M}/L = R\left(1 - \frac{1}{\sqrt{g(R)}}\right)\Big|_{R=1}, \qquad \mathcal{Q}/L = \frac{R^2 A_t'(R)}{2\sqrt{g(R)}f(R)}\Big|_{R=1}. \qquad (3.7)$$

The thermodynamic description of our solutions is complete after defining the chemical potential, temperature and entropy:

$$\mu = A(1) - A(R_+), \qquad T_H L = \lim_{R\to R_+} \frac{f'(R)}{4\pi\sqrt{f(R)g(R)}}, \qquad S/L^2 = \pi R_+^2, \qquad (3.8)$$

where we work in the gauge $A(R_+) = 0$. These quantities must satisfy the quasilocal form of the first law of thermodynamics:

$$\mathrm{d}\mathcal{M} = T_H\,\mathrm{d}S + \mu\,\mathrm{d}\mathcal{Q}, \qquad (3.9)$$

which is used to check our solutions.

As explained before, for reference we will often compare the hairy families of solutions against extremal RN BHs. RN BHs confined in a cavity can be parametrized by the horizon

---

[2]Note that the Maxwell term in action (3.1) is $\frac{1}{2}F^2$, not the perhaps more common F^2 term. It follows that the extremal RN BH satisfies the ADM relation $M = \sqrt{2}|Q|$, instead of $M = |Q|$ that holds when the Maxwell term in the action is F^2. Extremal RN BHs have $\mu = \sqrt{2}$ where μ is the chemical potential of the BH, and RN BHs exist for $0 < \mu \leq \sqrt{2}$.

[3]The Brown-York quasilocal quantities reduce to the ADM ones when we evaluate the former at $R \to \infty$.

radius R_+ and the chemical potential μ, and their quasilocal mass and charge are [26]

$$\mathcal{M}/L|_{RN} = 1 - \frac{\sqrt{2}(1-R_+)}{\sqrt{2-(2-\mu^2)R_+}}, \qquad \mathcal{Q}/L|_{RN} = \frac{\mu R_+}{\sqrt{2}\sqrt{2-(2-\mu^2)R_+}}. \tag{3.10}$$

where $0 < R_+ \leq 1$ (for the horizon to be confined inside the box) and $0 \leq \mu \leq \mu_{\text{ext}}$, with extremality reached at $\mu_{\text{ext}} = \sqrt{2}$. Note that at extremality one has $\mathcal{M}/L = R_+$ and $\mathcal{Q}/L = R_+/\sqrt{2}$. On the other hand, for any μ, when $R_+ = 1$ one has $\mathcal{M}/L = 1$ and $\mathcal{Q}/L = 2^{-1/2}$.

3.2 Description of the box: Israel junction conditions and stress tensor

So far, we discussed the boundary conditions at the horizon and asymptotic boundaries. However, hairy BHs are solutions that join an interior spacetime ($R < 1$; with superscript $^{\text{in}}$) with the known RN exterior background (3.5) ($R > 1$; with superscript $^{\text{out}}$). So, in practice we simply need to find the interior solution. For that, we need to integrate our equations of motion in the domain $R \in [R_+, 1]$. Therefore, we must specify appropriate conditions at the outer boundary of our integration domain, *i.e.* at $R = 1$. Next, we detail the procedures required to do this.

At and outside the box, *i.e.* for $R \geq 1$, the scalar field must vanish. However, its derivative when approaching the cavity from inside, *i.e.* as $R \to 1^-$, is finite (except for the trivial RN solution) and we will label this quantity ϵ:[4]

$$\phi^{\text{in}}|_{R=1} = \phi^{\text{out}}|_{R=1} = 0, \qquad \phi^{\text{out}}(R) = 0, \qquad \phi'^{\,\text{in}}|_{R=1} \equiv \epsilon. \tag{3.11}$$

That is, inside the box the scalar field is forced to have the Taylor expansion $\phi|_{R=1^-} = \epsilon(R-1) + \mathcal{O}\left((R-1)^2\right)$. We are forcing a jump in the derivative of the scalar field normal to the cavity timelike hypersurface Σ. This can be done only if we further impose junction conditions at Σ on the gravitoelectric fields as discussed next.

The box is the timelike hypersurface $\Sigma = R - 1 = 0$. It has outward unit normal $n_\mu = \partial_\mu \Sigma / |\partial \Sigma|$ ($n_\mu n^\mu = 1$) and coordinates $\xi^a = (\tau, \theta, \varphi)$. An observer in the interior of Σ measures the time $T^{\text{in}}(\tau) = \tau$ and the induced line element and gauge 1-form at Σ are

$$ds^2|_{\Sigma^{\text{in}}} = h_{ab}^{\text{in}} d\xi^a d\xi^b = -f^{\text{in}}|_{R=1} d\tau^2 + d\Omega_2^2\,,$$
$$A_t|_{\Sigma^{\text{in}}} = a_a^{\text{in}} d\xi^a = A_t^{\text{in}}|_{R=1} d\tau\,, \tag{3.12}$$

where h_{ab}^{in} is the induced metric in Σ and a_a^{in} is the induced gauge potential in Σ. Meanwhile, from the perspective of an observer outside the cavity, Σ is parametrically described by $R = 1$ and $T^{\text{out}}(\tau) = N\tau$ (so, N is a reparametrization freedom parameter) so that the induced line element and gauge 1-form for this observer are

$$ds^2|_{\Sigma^{\text{out}}} = h_{ab}^{\text{out}} d\xi^a d\xi^b = -N^2 f^{\text{out}}|_{R=1} d\tau^2 + d\Omega_2^2\,,$$
$$A_t|_{\Sigma^{\text{out}}} = a_a^{\text{out}} d\xi^a = N A_t^{\text{out}}|_{R=1} d\tau\,, \tag{3.13}$$

---

[4]Our theory has the symmetry $\phi \to -\phi$ so we can focus our attention only on the case $\epsilon > 0$.

Ideally, we would like to have a smooth crossing of Σ, whereby the induced gravitational h_{ab} and gauge a_a fields and their normal derivatives are continuous across Σ. That is to say, the Israel junction conditions should be obeyed [14–17]:

$$a_a^{\text{in}}\big|_{R=1} = a_a^{\text{out}}\big|_{R=1}\,, \tag{3.14a}$$

$$h_{ab}^{\text{in}}\big|_{R=1} = h_{ab}^{\text{out}}\big|_{R=1}\,; \tag{3.14b}$$

$$f_{aR}^{\text{in}}\big|_{R=1} = f_{aR}^{\text{out}}\big|_{R=1}\,, \tag{3.14c}$$

$$K_{ab}^{\text{in}}\big|_{R=1} = K_{ab}^{\text{out}}\big|_{R=1}\,; \tag{3.14d}$$

where $h_{ab} = g_{ab} - n_a n_b$ is the induced metric at Σ and $K_{ab} = h_a{}^\mu h_b{}^\nu \nabla_\mu n_\nu$ is the extrinsic curvature.

In the absence of the scalar condensate, we can set $N = 1$ and all the junction conditions (3.14) are satisfied. However, our hairy solutions are continuous but not differentiable at $R = 1$: they satisfy the conditions (3.14a)–(3.14c) but not (3.14d). Since the extrinsic curvature condition is violated, our hairy solutions are singular at Σ. But this singularity simply signals the presence of a Lanczos-Darmois-Israel surface stress tensor $\mathcal{S}_{ab}$ at the hypersurface layer proportional to the difference of the extrinsic curvature across the hypersurface [14–17]:

$$\mathcal{S}_{ab} = -\frac{1}{8\pi}\Big([K_{ab}] - [K]h_{ab}\Big), \tag{3.15}$$

where K is the trace of the extrinsic curvature and $[K_{ab}] \equiv K_{ab}^{\text{out}}\big|_{R=1} - K_{ab}^{\text{in}}\big|_{R=1}$. This surface tensor is the pull-back of the energy-momentum tensor integrated over a small region around the hypersurface Σ, *i.e.* it is obtained integrating the appropriate Gauss-Codazzi equation [14–17, 48]. It is also given by the jump across Σ of the Brown-York surface tensor [29] (see also discussion in [26]). Essentially, (3.15) describes the energy-momentum tensor of the cavity (the "internal structure" of the box) that is needed to confine the scalar field. Since the two Maxwell junction conditions (3.14a)–(3.14b) are satisfied, our hairy solutions will have a surface layer with no electric charge.

The strategy to find the hairy BHs of the theory can now be outlined. The hairy solution inside the box is found integrating numerically the coupled system of three ODEs in the domain $R \in [R_+, 1]$. This is done while imposing the boundary conditions (3.3) at the horizon and, at the box, we impose $\phi(1^-) = 0$ and use the scaling symmetry (3.4) to set $f(1^-) = 1$. After this task, we can compute the quasilocal charges (3.7) and the other thermodynamic quantities (3.8) of the system. To find the solution in the full domain $R \in [R_+, \infty]$ we impose the three junction conditions (3.14a)–(3.14c) at the box to match the interior solution with the outer solution (described by the RN solution (3.5)). This operation finds the parameters M_0, C_A, ρ in (3.5) as a function of the reparametrization freedom parameter N introduced in (3.13). The Israel stress tensor $\mathcal{S}_a^b$ is just a function of N and, if $\phi^{\text{in}} \neq 0$, we cannot choose N to kill all the components of $\mathcal{S}_a^b$ (there are two non-vanishing components, $\mathcal{S}_t^t$ and $\mathcal{S}_\theta^\theta = \mathcal{S}_\varphi^\varphi$). In this process, we have arbitrary freedom to choose N. This simply reflects the freedom we have to select the energy-momentum content of the box needed to confine the scalar condensate. We should however, make a selection

that respects some or all the energy conditions [18]. Once this choice is made, we can finally compute the ADM mass and charge (3.6) of the hairy solution which, necessarily, includes the contribution from the box.

3.3 Numerical scheme

The hairy BHs we seek are a 2-parameter family of solutions, that we can take to be the horizon radius R_+ and the scalar field amplitude $\epsilon \equiv \phi'(R = 1)$ as defined in (3.11). In practice, we set up a two dimensional discrete grid where we march our solutions along these two parameters. In other words, we give R_+ and ϵ as inputs of our numerical code, and in the end of the day we read the horizon parameters f_0, A_0, ϕ_0 in (3.3), and the values of the derivative of f and the value of A and its derivative at the box, $R = 1$. Typically, we start near the merger with the RN BH where a good seed (approximation) for the Newton-Raphson method we use is the RN BH itself but with a small perturbation that also excites the scalar field.

We find it convenient to introduce a new radial coordinate

$$y = \frac{R - R_+}{1 - R_+} \tag{3.16}$$

so that the event horizon is at $y = 0$ and the box at $y = 1$. The equations of motion now depend explicitly on R_+.

Moreover, we also find useful to redefine the fields as

$$f = y\, q_1(y), \qquad A = y\, q_2(y), \qquad \phi = -(1 - y)\, q_3(y) \tag{3.17}$$

which automatically imposes the boundary conditions (3.3) at the horizon. We now use the scaling symmetry (3.4) to set $f(1^-) = 1$ and introduce the scalar amplitude (3.11) at the box. This can be done through imposing the boundary conditions

$$q_1(1) = 1, \qquad q_3(1) = \epsilon. \tag{3.18}$$

The other boundary conditions for $q_{1,2,3}$ are derived boundary conditions in the sense that they follow directly from evaluating the equations of motion at the boundaries $y = 0$ and $y = 1$ [49]. Under these conditions, the hairy BHs are described by smooth functions $q_{1,2,3}$ that we search for numerically.

To solve numerically our boundary value problem, we use a standard Newton-Raphson algorithm and discretise the coupled system of three ODEs using pseudospectral collocation (with Chebyshev-Gauss-Lobatto nodes). The resulting algebraic linear systems are solved by LU decomposition. These numerical methods are described in detail in the review [49]. Since we are using pseudospectral collocation, and our functions are analytic, our results must have exponential convergence with the number of grid points. We check this is indeed the case and the thermodynamic quantities that we display have, typically, 8 decimal digit accuracy. We further use the quasilocal first law (3.9) (typically, obeyed within an error smaller than $10^{-3}\%$) to check our solutions.

4 Phase diagram of the charged black hole bomb system

The properties of the hairy black holes of the charged black hole bomb system are closely linked to the superradiant/near-horizon instability of RN black holes,[5] so we first highlight some features of this instability to provide the context needed to interpret the hairy black hole phase diagram (see [21] for details).

In the left panel of figure 1 we sketch (from [21]) the scalar field instability onset charge $e_{\mathrm{onset}} = q_{\mathrm{onset}}L$ as a function of R_+ for three families of RN black holes with constant chemical potential μ, *i.e.* the minimum scalar charge needed for a black hole with (R_+, μ) to be unstable. We can see that the near-horizon charge e_{NH} is a lower bound for an RN instability, *i.e.* caged RN BHs are always stable when $e < e_{\mathrm{NH}}$. Correspondingly, we also find no hairy black holes when $e < e_{\mathrm{NH}}$. At the other end, all extremal RN black holes, no matter their R_+, are unstable at or above the superradiant charge e_{S}. In between these two critical charges $e_{\mathrm{NH}} < e < e_{\mathrm{S}}$ we have a window of horizon radii $R_+ \in [R_+|_P, 1]$ within which sufficiently near-extremal RN black holes are unstable. In equivalent words, for $e_{\mathrm{NH}} < e < e_{\mathrm{S}}$, extremal RN BHs are unstable for quasilocal charges in the range $\mathcal{Q}/L \in [(\mathcal{Q}/L)|_P, 2^{-\frac{1}{2}}]$. In the upcoming phase diagrams we will indicate the instability onset curve as a yellow curve $P\alpha$ and, when applicable, we will also use a gold diamond point P to identify the minimum charge for instability. The onset curve starts at point P where it intersects the extremal RN curve and terminates at point α with $\mathcal{Q}/L = 2^{-\frac{1}{2}}$ (*i.e.* $R_+ = 1$) where it intersects again the extremal RN curve.

In all our plots $\mathcal{M}$ and $\mathcal{Q}$ are the Brown-York quasilocal mass and charge (3.7) of the system, measured at the location of the box. Different solutions tend to pile-up in certain regions of the $\mathcal{Q}$-$\mathcal{M}$ diagram (as illustrated in figure 10). Thus, the distinction between different solutions becomes clearer if we use instead $\Delta\mathcal{M} = \mathcal{M} - \mathcal{M}|_{\mathrm{ext\,RN}}$ which is the quasilocal mass difference of a hairy solution with an extremal RN that has the *same* quasilocal charge $\mathcal{Q}$. Thus, in our $\mathcal{Q}$-$\Delta\mathcal{M}$ plots, the horizontal orange line $O\alpha$ with $\Delta\mathcal{M} = 0$ describes the extremal RN BH. It is constrained to have $\mathcal{Q}/L \leq 2^{-\frac{1}{2}}$ (point α) in order to fit inside the box (this extremal line will be represented by a dark red line in the 3-dimensional plots $\mathcal{Q}$-$\Delta\mathcal{M}$-S).

From the RN quasilocal charges (3.10), in the quasilocal $\mathcal{Q} - \mathcal{M}$ plot, the region that represents RN BHs with horizon radius inside the box is the triangular surface bounded by the lines $\mathcal{Q} = 0$, $\mathcal{M} = \sqrt{2}\mathcal{Q}$ and $\mathcal{M}/L = 1$. Therefore, in the $\mathcal{Q} - \Delta\mathcal{M}$ plane, non-extremal RN BHs with $R_+ \leq 1$ are those inside the triangular region bounded by $\mathcal{Q} = 0$, $\Delta\mathcal{M} = 0$ and $\Delta\mathcal{M}/L = 1 - \sqrt{2}\mathcal{Q}/L$. The boundary $\mathcal{Q} = 0$ describes the Schwarzschild limit, $\Delta\mathcal{M} = 0$ is the extremal RN boundary and the latter curve is

$$(\mathcal{Q}/L, \Delta\mathcal{M}/L) = \left(L^{-1}\mathcal{Q}|_{\mathrm{ext\,RN}}, 1 - L^{-1}\mathcal{M}|_{\mathrm{ext\,RN}}\right) = \left(\frac{R_+}{\sqrt{2}}, 1 - R_+\right) \qquad (4.1)$$

where $\mathcal{M}|_{\mathrm{ext\,RN}}$ and $\mathcal{Q}|_{\mathrm{ext\,RN}}$ are given by (3.10) with $\mu = \mu_{\mathrm{ext}} = \sqrt{2}$. The red dashed line in the forthcoming $\mathcal{Q} - \Delta\mathcal{M}$ plots is this parametric curve (4.1) with R_+ *allowed*

---

[5]For a general RN black hole the superradiant and near-horizon instabilities are entangled, so we will simply refer to an RN instability, regardless of the origin.

to take also values above 1. Indeed, it turns out that the most charged solutions we find approach this dashed red line (4.1) (in the limit where scalar condensate amplitude approaches infinity). In this sense, for a given quasilocal mass (smaller than 1), this red dashed line (4.1) represents the maximal quasilocal charge that confined solutions can have, with or without scalar hair.

As discussed in our summary of results (section 2), the charged black hole bomb system has a total of four critical scalar field charges. Besides $e_{\mathrm{NH}} = \frac{1}{2\sqrt{2}} \sim 0.354$ and $e_{\mathrm{S}} = \frac{\pi}{\sqrt{2}} \sim 2.221$ discussed above, the two others are $e_\gamma \sim 1.13$ and $e_c \sim 1.8545 \pm 0.0005$. Accordingly, the phase diagram of hairy boson stars and hairy black holes depends on the value of e compared to these four fundamental critical charges of the system. Thus, in the next subsections, we describe the properties of hairy solutions in the following four windows of scalar field charge: 1) $e_{\mathrm{NH}} \leq e < e_\gamma$, 2) $e_\gamma \leq e \leq e_c$, 3) $e_c \leq e < e_{\mathrm{S}}$, and 4) $e \geq e_{\mathrm{S}}$. For concreteness, we will display results for a representative value of e for each one of these windows, namely: 1) $e = 1$ (section 4.1), 2) $e = 1.85$ (section 4.2), 3) $e = 2$ (section 4.3), and 4) $e = 2.3$ (section 4.4). Altogether, these results (and others not presented) will allow us to extract the conclusions summarized in section 2.

4.1 Phase diagram for $e_{\mathrm{NH}} \leq e < e_\gamma$

The left panel of figure 3 is the phase diagram $\mathcal{Q}$-$\Delta\mathcal{M}$ for $e = 1$, representative of the range $e_{\mathrm{NH}} \leq e < e_\gamma$. The black disk curve describes the only family of boson stars of the theory for this (range of) e which is the main/perturbative family. This corresponds to the black curve $OABC\cdots$ (already present for $e < e_{\mathrm{NH}}$) with its Chandrasekhar limit A and a series of cusps $A, B, C, \cdots$ and associated zig-zagged branches sketched in the top-left panel of figure 2. The properties of this boson star were already studied in much detail in [28] so we do not expand further. Our interest here are the hairy BHs.

The horizontal orange curve $OP\alpha$ with $\Delta\mathcal{M} = 0$ is the extremal RN BH family with $\mathcal{Q}/L \leq 2^{-\frac{1}{2}}$ and boxed non-extremal BHs exist above this line and to the left of the red dashed line (4.1) to fit inside the cavity, as detailed above. The yellow curve $P\alpha$, that intersects and terminates at the extremal RN curve precisely at P and α, describes the instability onset curve of RN BHs as computed using linear analysis in [21]. It coincides with the merger line of hairy BHs with RN BHs, as it had to. Indeed, recall that hairy BHs can be parametrized by their horizon radius R_+ and the scalar field amplitude ϵ. When $\epsilon = 0$ we recover the 1-parameter family $P\alpha$ of RN BHs at the onset of the instability. RN BHs are unstable below this onset curve $P\alpha$ all the way down to the horizontal extremal line also labelled $P\alpha$. This region is extremely small for this value of e but it will be wider as e increases.

Hairy BHs (blue circles) exist inside the closed line $P\alpha\beta$. That is, they exist below the onset curve $P\alpha$ and to the left of the red $\alpha\beta$ dashed line (4.1), all the way down till they reach a line $P\beta$ where the Kretschmann curvature scalar evaluated at the horizon $K|_{\mathcal{H}} = R_{abcd}R^{abcd}|_{R_+}$ grows large without bound. This occurs at finite R_+ and thus at *finite entropy* $S/L^2 = \pi R_+^2$, and the *temperature vanishes* along this boundary curve $P\beta$. The entropy is however not constant along this singular extremal boundary curve (in practice, the last curve we plot has $R_+ = 0.1$ but it should extend a bit further down in
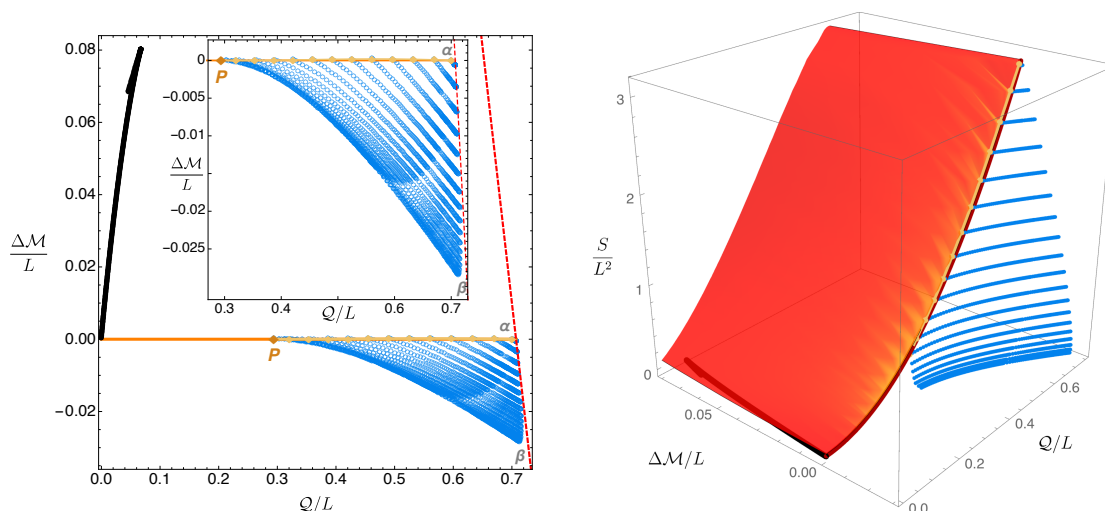
Figure 3. Phase diagrams for Einstein-Maxwell theory with a scalar field charge $e = 1$ ($e_{\rm NH} \leq e < e_\gamma$) in a Minkowski box. *Left panel:* quasilocal mass difference $\Delta\mathcal{M}/L$ as a function of the quasilocal charge $\mathcal{Q}/L$. The black disk curve is the main/perturbative soliton family, the orange line is the extremal RN BH (RN black holes exist above it), and the blue circles describe hairy black holes. The yellow curve is the superradiant onset curve of RN (just above but very close to the extremal RN curve with the two merging at P and α). It agrees with the hairy solutions in the limit where these have $\epsilon = 0$ (no scalar condensate) and thus merge with RN family. The red dashed line with negative slope signals solutions with $\Delta\mathcal{M}/L = 1 - \sqrt{2}\mathcal{Q}/L$ i.e. black holes with horizon radius $R_+ = 1$ (above this value they do not fit inside the cavity). *Right panel:* dimensionless entropy S/L^2 as a function of the quasilocal charge and mass difference. RN BHs are the two parameter red surface with extremality described by the 1-parameter curve $\Delta\mathcal{M} = 0$ (dark red). The instability onset is described by the yellow curve (very close to extremality) and RN between these two curves are unstable. When they coexist with RN BHs, for a given $(\mathcal{Q}, \mathcal{M})/L$, hairy BHs (blue dots) always have more entropy than RN, *i.e.* they dominate the microcanonical ensemble. For $e_{\rm NH} \leq e < e_\gamma$, hairy BHs terminate at an extremal BH (*i.e.* with zero temperature) and finite entropy (and divergent horizon curvature). The soliton (black dots) with zero entropy is also shown.

the region close to $\alpha\beta$). We typically find that lines of constant R_+ extend all the way to the red $\alpha\beta$ dashed line (4.1), but the latter is only reached in the limit $\epsilon \to \infty$. This makes it harder to extend our solution to regions even closer to $\alpha\beta$ (a fixed step in ϵ corresponds to an increasingly smaller progression in $\mathcal{Q}$ as $\alpha\beta$ is approached). Hairy BHs do not exist for $\mathcal{Q} < \mathcal{Q}|_P$, in agreement with the linear analysis of the left panel of figure 1, and there is clearly no relation between the hairy BHs and the boson star of the theory when $e = 1$ and, more generically, for $e_{\rm NH} \leq e < e_\gamma$.

Because point P does not coincide with the origin O, hairy BHs with $e_{\rm NH} \leq e < e_\gamma$ were not found in the perturbative analysis of [26]. Indeed, this perturbative analysis only captures hairy BHs that have small mass and charge.

The right panel of figure 3 plots the same phase diagram as the left panel but this time with the entropy S/L^2 on the extra vertical axis. The latter is the appropriate thermodynamic potential to discuss the preferred thermal phases of the microcanonical

ensemble: for a given quasilocal mass $\mathcal{M}/L$ and charge $\mathcal{Q}/L$ fixed, the dominant phase is the one with the largest entropy. The red surface represents (a subset[6]) of RN BHs, both stable and unstable with the boundary line of stability being again the yellow dotted curve, here very close to the extremal RN BH (dark red with $\Delta\mathcal{M} = 0$). In the $S = 0$ plane we find the perturbative boson star (black curve). The blue dots fill the 2-dimensional surface that describe hairy BHs (which merge with RN along the yellow line). Again we see (not very clearly but it will be more clear for higher e) that hairy BHs coexist with RN black holes in the region between the onset and extremal RN curves. In this case, we find that hairy black holes always have a larger entropy than the corresponding RN BHs with same $\mathcal{M}/L$ and $\mathcal{Q}/L$. So they are the thermodynamically preferred phase in the microcanonical ensemble.

Hence, it follows from the second law of thermodynamics that hairy BHs with $(\mathcal{Q}, \mathcal{M})$ between the RN onset and extremality curves are natural candidates for the endpoint of the RN superradiant/near-horizon instability when we do a time evolution of the instability where we preserve the mass and charge of the system.

4.2 Phase diagram for $e_\gamma \leq e < e_c$

In figure 4 we display the phase diagram when $e = 1.85$, which is representative of the range $e_\gamma \leq e < e_c$ that we sketched in the top-right panel of figure 2. As a first observation we note that, besides the main or perturbative boson star family (black curve) already present for $e < e_\gamma$, the diagram now also has the magenta line that starts at finite $\mathcal{Q}$, passes though point $\star$, and terminates at point β on the red dashed line. This is the secondary or non-perturbative family of boson stars. On its left side, this family has itself a series of cusps and zig-zagged secondary branches denoted as $B, C, \cdots$ in the sketch of the top-right panel of figure 2 (not displayed in figure 4). These details are not relevant here, and we ask the reader to see [28] for an exhaustive study of boson stars' properties. It is however important to emphasize that this secondary/non-perturbative family exists (as a ground state family) only for $e_\gamma \leq e < e_c$, thus explaining the origin of the critical charges e_γ and e_c. At $e = e_c$ the magenta line of figure 4 merges with the black line (see section 4.3). On the other hand, as we decrease e below e_c one finds that the gap $\Delta\mathcal{Q}$ between the black and magenta families increases, and the "length" of the magenta line decreases because the left endpoint of this curve approaches β. It keeps doing so till it only exists on a very small neighbourhood of the red dashed line and, at $e = e_\gamma$, this line shrinks to the single point β. Below e_γ, the non-perturbative family ceases to exist (as seen in section 4.1). Essentially because it no longer fits inside the cavity. This discussion is better illustrated in the right panel of figure 1: 1) if we collect all non-perturbative solitons in a single plot, we find that they exist only in the window $e_\gamma \leq e < e_c$ and they fill the area bounded by the auxiliary dashed lines $a_c\beta_c\gamma$; 2) very close to e_c the non-perturbative soliton is almost on top of the auxiliary curve $a_c\beta_c$; and 3) on the opposite end, as $e \to e_\gamma$, the perturbative soliton line shrinks to the point γ on the red dashed line.

What are the consequences of these boson star discussions for the hairy BHs? Hairy BHs with $e = 1.85$ are the blue circles in figure 4. As before, they exist in the area

---

[6]We just plot the portion of the RN surface with $\Delta\mathcal{M} < 0.085$ that covers the region where the boson star also exists.
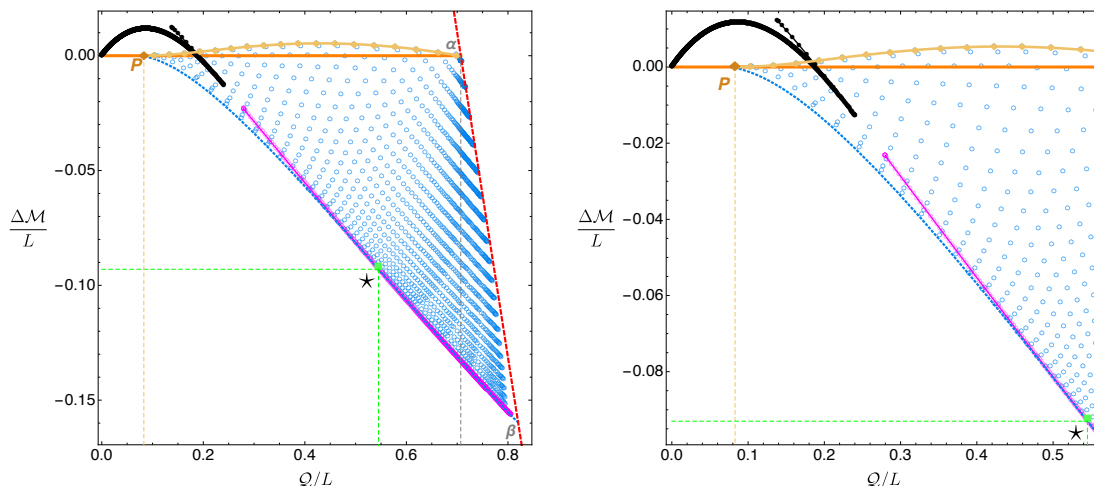
Figure 4. Phase diagram for Einstein theory with a scalar field charge $e = 1.85$ ($e_\gamma \leq e < e_c$) in a Minkowski box. The blue circles describe hairy black holes, the black disk (magenta circle) curve is the soliton main (secondary) family, and the orange line is the extremal RN BH (non-extremal RN BHs exist above it). The yellow curve is the superradiant onset curve of RN. As it could not be otherwise, it agrees with the hairy solutions in the limit where these have $\epsilon = 0$ and thus merge with RN family. The dashed vertical line is at $\mathcal{Q} = 2^{-1/2}$ which is the maximum local charge that an extremal RN BH can have while fitting inside a box with radius $R = 1$. The red dashed line (4.1) describes the boundary for black holes that can fit inside the cavity with radius $R = 1$. The green solid square labelled with a star ($\star$) has $(\mathcal{Q}_\star, \mathcal{M}_\star, \Delta\mathcal{M}_\star) \sim (0.545, 0.678, -0.093)$. The auxiliary blue dotted curve $P \star \beta$ in the bottom describes the line where hairy BHs terminate with unbounded horizon curvature. Hairy BHs that terminate in the trench $P\star$ of this auxiliary curve do so at finite entropy and vanishing temperature. On the other hand, hairy BHs that terminate in the trench segment $\star\beta$ (that coincides with magenta soliton line) do so at zero entropy and large (possibly infinite) temperature.
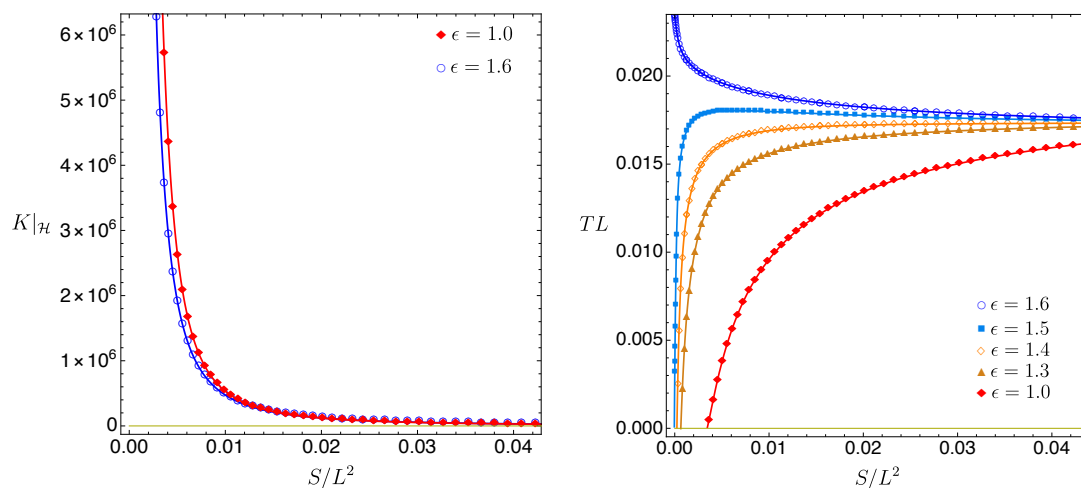

Figure 5. Kretschmann curvature at the horizon (left panel) and temperature (right panel) as a function of the entropy ($S/L^2 = \pi R_+^2$) for several hairy BH families with constant scalar amplitude ϵ and scalar field charge $e = 1.85$ ($e_\gamma \leq e < e_c$).
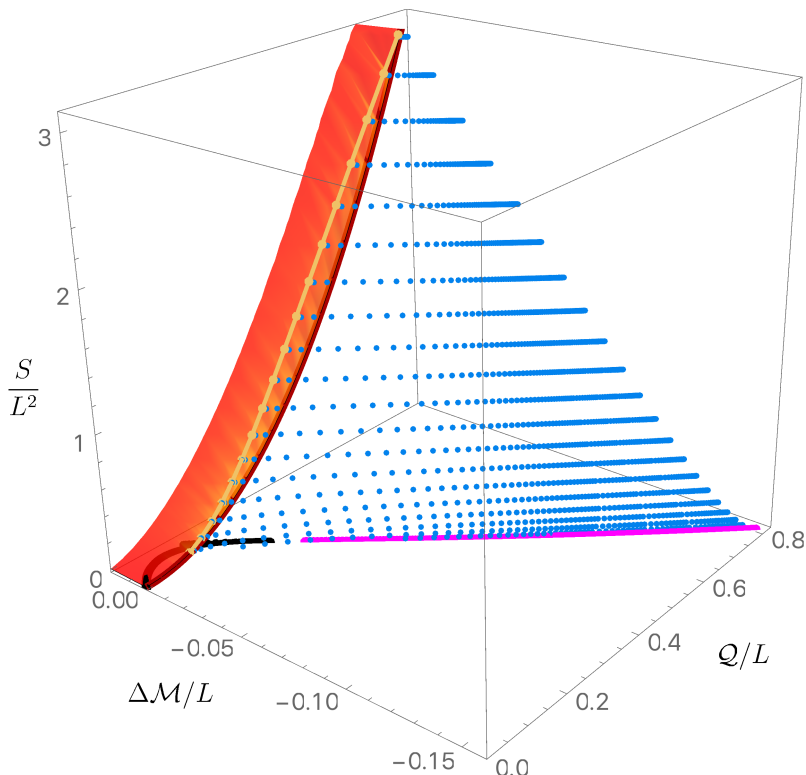
Figure 6. Entropy as a function of the quasilocal charge and mass difference for Einstein theory with a scalar field charge $e = 1.85$ ($e_\gamma \leq e < e_c$) in a Minkowski box. The red surface represents RN BHs in the range $0 \leq \Delta\mathcal{M} < 0.02$ (they extend for higher $\Delta\mathcal{M}$) with the dark red line with $\Delta\mathcal{M} = 0$ being the extremal RN BH family. The yellow line describes the merger line between RN BHs and hairy BHs, and RN BHs between this line and the dark red extremal line are unstable. The blue disks describe hairy BHs and the black (magenta) lines with $S = 0$ describe the main (secondary) soliton family. When they coexist with RN BHs, for a given $(\mathcal{Q}, \mathcal{M})/L$, hairy BHs always have more entropy than RN, *i.e.* they dominate the microcanonical ensemble.

bounded by $P\alpha\beta$, where $P\alpha$ is the merger yellow line with RN BHs and coincides with the instability onset curve of [21], and $\alpha\beta$ is a segment of the red dashed line (4.1). Starting at the onset curve $P\alpha$ and moving down, *e.g.* along constant $\mathcal{Q}$ lines, we find that hairy BHs terminate at the line $P\beta$ (or $P \star \beta$). This is the blue dashed line in figure 4 which describes hairy BHs with minimum entropy/horizon radius for a given charge. Along this line, the Kretschmann curvature scalar evaluated at the horizon $K|_\mathcal{H}$ grows very large (most probably, $K|_\mathcal{H} \to \infty$). To illustrate this, in the left panel of figure 5 we plot $K|_\mathcal{H}$ as a function of the entropy $S/L^2 = \pi R_+^2$ as we approach the line $P\beta$ (at small S) along curves of constant scalar amplitude ϵ (shown in the legends). Indeed, for small S/L^2 the curvature is growing very large.

So far the phase diagram of hairy BHs looks similar to the one for $e_{\mathrm{NH}} \leq e < e_\gamma$ (section 4.1). However, for $e_\gamma \leq e < e_c$ we now find that the way hairy BHs terminate along the singular curve differs substantially depending on whether it ends to the left or to the right of the green square point $\star$ in figure 4 (with $\mathcal{Q}_\star/L \simeq 0.545$ for $e = 1.85$). When

the hairy BHs terminate along $P\star$, they do so at *finite entropy* and *vanishing temperature*. On the other hand, hairy BHs that terminate along $\star\beta$ do so at *vanishing entropy* and *large (possibly infinite) temperature*. To illustrate this, in the right panel of figure 5 we plot the temperature TL as a function of the entropy $S/L^2 = \pi R_+^2$ as we follow hairy BH families that approach the singular line $P\beta$ at (different; see legends) constant scalar amplitude ϵ. Point $\star$ has $(\mathcal{Q}_\star, \Delta\mathcal{M}_\star) \sim (0.545, -0.093)$ which corresponds to $(R_+, \epsilon)\big|_\star = (0, 1.55 \pm 0.05)$. Hairy BHs with $\epsilon < \epsilon_\star$ terminate at $P\star$, while hairy BHs with $\epsilon > \epsilon_\star$ end at $\star\beta$. The right panel of figure 5 indeed shows that hairy BHs with $\epsilon < \epsilon_\star$ approach $P\star$ at finite S/L^2 and with $TL \to 0$ (like all hairy BHs of section 4.1), while those with $\epsilon > \epsilon_\star$ approach $\star\beta$ with $S \to 0$ and $TL \to \infty$.

Another important conclusion that emerges from figure 4, is that hairy BHs which have a zero horizon radius limit terminate precisely along the segment $\star\beta$ of the secondary/non-perturbative soliton family. This means that hairy BHs terminate with the *same* $\mathcal{Q}$ and $\mathcal{M}$ as the non-perturbative soliton (but the gravitoelectric and scalar fields of the two solutions are different). On the other hand, those that end at $P\star$ do so in a manner that is very similar to the way the hairy BHs with $e_{\mathrm{NH}} \leq e < e_\gamma$ terminate (section 4.1).

We find that the critical charge $\mathcal{Q}_\star(e)$ decreases as e grows from e_γ till e_c. As explained when discussing the right plot of figure 1, the non-perturbative soliton line shrinks to the point β when $e \to e_\gamma$. Thus, our expectation is that the critical charge $\mathcal{Q}_\star$ also reaches $\mathcal{Q}\big|_\beta$ when $e \to e_\gamma^+$. That is to say, we expect that hairy black holes are connected to the non-perturbative soliton as soon as it exists. However, determining numerically $\mathcal{Q}_\star$ in this limit is very difficult, since hairy BHs near β have very large values of ϵ.

The hairy BHs with $e_\gamma \leq e < e_c$ we find were not captured by the perturbative analysis of [26] because they do not extend to arbitrarily small mass and charge.

In figure 6, we plot the thermodynamic potential of the microcanonical ensemble — the entropy S/L^2 — as a function of $\mathcal{Q}$ and $\Delta\mathcal{M}$. In the $S = 0$ plane we find the perturbative boson star (black curve) and, for larger $\mathcal{Q}$ and after a gap, the non-perturbative boson star (magenta curve). As before, the red surface describes the RN BH family parametrized by R_+ and μ as in (3.10) and with $S/L^2 = \pi R_+^2$. It terminates at the dark red extremal curve with $\Delta\mathcal{M} = 0$. We only plot the portion of the RN surface with $\Delta\mathcal{M} < 0.02$ that covers the region where the perturbative boson star also exists. Unstable RN BHs are those between the instability onset (yellow dotted curve) and the extremal RN dark red curve. The blue dots fill the 2-dimensional surface that describes hairy BHs. It merges with RN BHs along the yellow dotted curve and then extends to lower $\Delta\mathcal{M}$ with an entropy that is always larger the RN BH with the same $\mathcal{Q}$ and $\mathcal{M}$ (when they coexist). Therefore, hairy BHs are the thermodynamically dominant phase in the microcanonical ensemble. Consequently, from the second law of thermodynamics, hairy BHs with $(\mathcal{Q}, \mathcal{M})$ between the RN onset and extremality curves are candidates for the endpoint of the RN superradiant/near-horizon instability when in a time evolution of the RN instability at constant mass and charge.

4.3 Phase diagram for $e_c \leq e < e_{\mathrm{s}}$

In figure 7 we give the phase diagram for $e = 2$. This is the case we choose to illustrate the solution spectra in the range $e_\gamma \leq e < e_c$ that we sketched in the bottom-left panel of
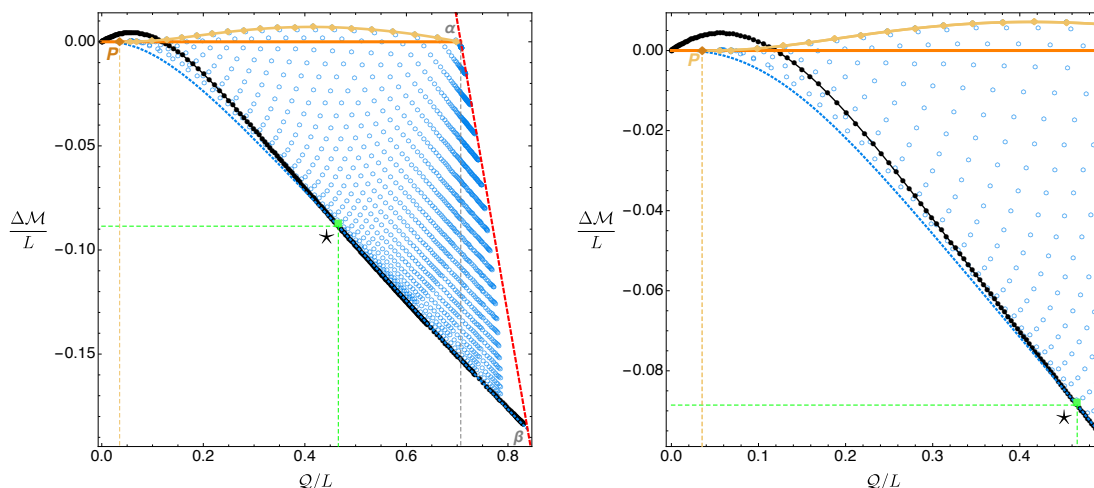
Figure 7. Phase diagram for Einstein theory with a scalar field charge $e = 2$ ($e_c \leq e < e_S$) in a Minkowski box. As before, the blue circles describe hairy black holes, the black disk curve is the soliton main family, and the orange line is the extremal RN BH (RN black holes exist above it). The gray and red dashed curves have the same interpretation as in figure 4. The green solid square labelled with a star ($\star$) has $(\mathcal{Q}_\star, \mathcal{M}_\star, \Delta\mathcal{M}_\star) \sim (0.466, 0.659, -0.0886)$. The auxiliary blue dotted curve $P \star \beta$ in the bottom describes the line where hairy BHs terminate with unbounded horizon curvature. Hairy BHs that terminate in the trench $P\star$ of this auxiliary curve have zero temperature ($T = 0$) and finite entropy $S/L = \pi R_+^2$. On the other hand, hairy BHs that terminate in the trench segment $\star\beta$ (that coincides with the black soliton line) have zero entropy and large (possibly infinite) temperature. Note that these $\star\beta$ terminal hairy BHs have the same $(\mathcal{Q}, \Delta\mathcal{M})$ as the main soliton family with $\mathcal{Q} > \mathcal{Q}_\star$.

figure 2. Comparing with the diagram of figure 4 we immediately notice that the magenta line representing the non-perturbative soliton family is no longer present in figure 7. This is because at $e = e_c$, the perturbative and non-perturbative boson star families (*i.e.* the black and magenta lines of figure 4) merge and for $e \geq e_c$ the main or perturbative boson star family no longer has a Chandrasekhar mass limit and now extends from the origin O all the way to β in the red dashed line. This merger at e_c occurs in an interesting elaborated manner. In particular, going back to top-right sketch of figure 2, at $e = e_c$ the secondary zig-zagged branches $\cdots CBA$ of the perturbative (black) soliton also merge with the secondary zig-zagged branches $abc\cdots$ of the non-perturbative (magenta) soliton. As a consequence, for $e \geq e_c$ there is also a secondary soliton $\cdots CBbc\cdots$ (purple line in bottom-left of figure 2) that has higher energy than the perturbative (black) soliton $P\beta$. This secondary family is not displayed in figure 7 because it plays no role on the discussion of hairy BHs of the theory. The reader can find a detailed discussion of soliton's properties across the transition at $e = e_c$ in [28].

Since the colour code and associated labelling in figure 7 is the same as in figures 3 and 4 we can now immediately discuss the hairy BHs. Again they exist in the area enclosed by $P\alpha\beta$ filled with the blue circles. They merge with the RN family along the yellow dotted line $P\alpha$ when the scalar condensate vanishes, which agrees with the RN instability curve found in [21]. The hairy BHs then exist all the way down to the blue dashed line $P\beta$ (or
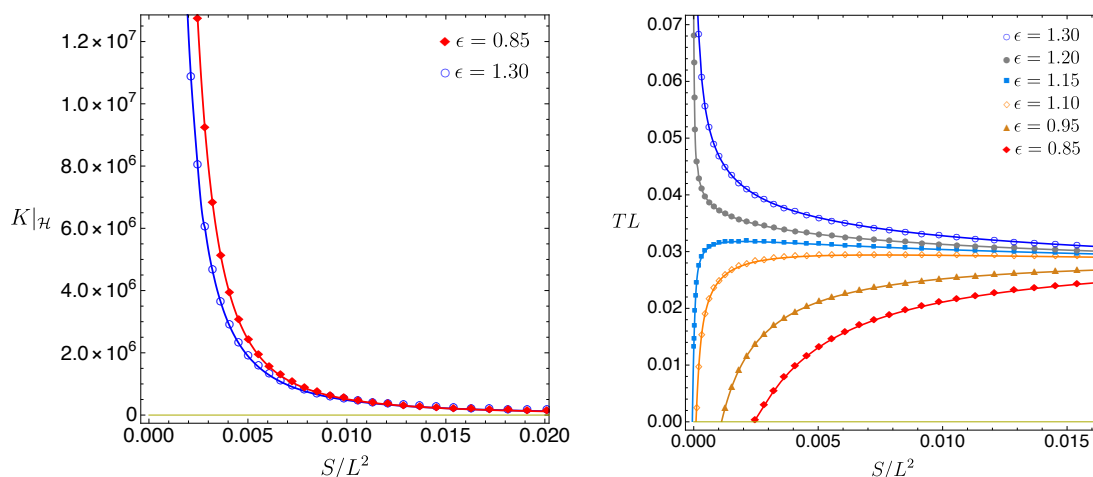
Figure 8. Kretschmann curvature at the horizon (left panel) and temperature (right panel) as a function of the entropy ($S/L^2 = \pi R_+^2$) for hairy BH families with fixed ϵ and scalar field charge $e = 2$ ($e_c \leq e < e_{\rm s}$).

$P\star\beta$) which, for a given charge, identifies the hairy BH that has minimum entropy/horizon radius. The Kretschmann curvature evaluated at the horizon $K|_{\mathcal{H}}$ diverges. For a given charge, $P\beta$ identifies the hairy BHs with minimum entropy/horizon radius and $K|_{\mathcal{H}}$ grows very large along it. This is confirmed in the left panel of figure 8: as we approach $P\beta$ (at small S) along lines of constant scalar amplitude ϵ (identified in the legends), $K|_{\mathcal{H}}$ is growing very large.

Point $\star$ with charge $\mathcal{Q}_\star \simeq 0.466$ describes a transition point. Hairy BHs that end to the left of this point along $P\star$ do so at finite S with $T \to 0$. However, one has $S \to 0$ and $T \to \infty$ when the hairy BHs terminate along $\star\beta$ with $\mathcal{Q} > \mathcal{Q}_\star$. This is confirmed in the right panel of figure 8 where we plot the temperature TL as a function of the entropy $S/L^2 = \pi R_+^2$ as we follow different families of constant scalar amplitude hairy BHs that approach the singular line $P\beta$. Point $\star$ has $(\mathcal{Q}_\star, \Delta\mathcal{M}_\star) \sim (0.466, -0.0886)$ which corresponds to $(R_+, \epsilon)|_\star = (0, 1.175 \pm 0.005)$. Hairy BHs with $\epsilon < \epsilon_\star$ have $\mathcal{Q} < \mathcal{Q}_\star$ and terminate at $P\star$, while hairy BHs with $\epsilon > \epsilon_\star$ have $\mathcal{Q} > \mathcal{Q}_\star$ and end at $\star\beta$.

From figure 7 and the right panel of figure 8, it should not go without notice that the hairy BHs that have a zero horizon radius limit terminate along the trench $\star\beta$ of the perturbative soliton family. That is, *when* the hairy BHs have zero entropy, they have the same charge $\mathcal{Q}$ and mass $\mathcal{M}$ as the perturbative soliton. In a nutshell, hairy BHs with $e_c \leq e < e_{\rm s}$ have a behaviour that is qualitatively similar to those of $e_\gamma \leq e < e_c$ (section 4.2). However, the zero entropy BHs now terminate on top of the perturbative soliton in the $\mathcal{Q}$-$\mathcal{M}$ phase diagram instead of ending on the non-perturbative soliton (which is now an excited solution $\cdots CBbc \cdots$ in the bottom-left panel of figure 2). We also find that the critical charge $\mathcal{Q}_\star(e)$ decreases and approaches $\mathcal{Q}_P$ as e grows from e_c to $e_{\rm s}$. Moreover, we find that $\mathcal{Q}_\star \to \mathcal{Q}_P \to 0$ as $e \to e_{\rm s}$.

Figure 9, displays the phase diagram of the microcanonical ensemble for $e = 2$: the entropy S/L^2 as a function of $\mathcal{Q}$ and $\Delta\mathcal{M}$. The colour code of this diagram is the same
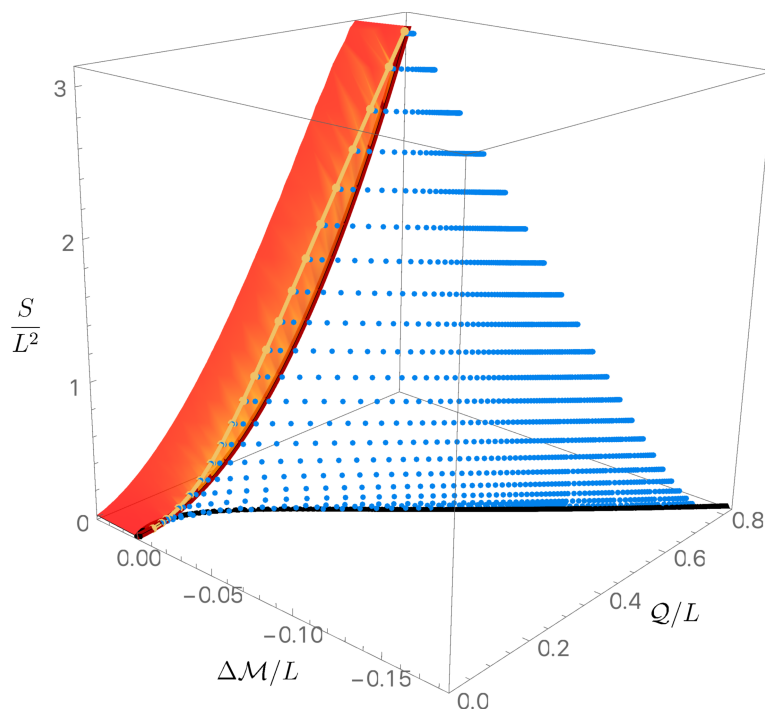
Figure 9. Entropy as a function of the quasilocal charge and mass difference for Einstein theory with a scalar field charge $e = 2$ ($e_c \leq e < e_{\rm S}$) in a Minkowski box. When they coexist with RN BHs, for a given $(\mathcal{Q}, \mathcal{M})/L$, hairy BHs always have more entropy than RN, *i.e.* they dominate the microcanonical ensemble. For $e_c \leq e < e_{\rm S}$, when $\mathcal{Q} > \mathcal{Q}_{\star}(e)$, hairy BHs have a zero entropy limit where they coincide with the soliton (black disk) curve in the sense that they have the same $(\mathcal{Q}, \mathcal{M})/L$ as the soliton (the temperature and horizon curvature diverges). However, when $0 < \mathcal{Q} < \mathcal{Q}_{\star}(e)$, hairy BHs terminate at an extremal BH (*i.e.* with zero temperature) and finite entropy (and divergent horizon curvature) along a line that does not coincide with the black disk one for the soliton.

as figure 6. Because e is bigger than the cases considered before, we see that the region between the onset yellow curve and the extremal RN dark red curve where RN BHs are unstable is now quite visible. Again we find that the hairy BHs (blue circles) that bifurcate from the yellow onset curve always have higher entropy that the RN BHs with the same $(\mathcal{Q}/L, \mathcal{M}/L)$ when they coexist. It follows that also for $e_c \leq e < e_{\rm S}$, hairy BHs are the preferred thermodynamic phase in the microcanonical ensemble. As expected from figure 7, for $\mathcal{Q} \geq \mathcal{Q}_{\star} \simeq 0.466$, the hairy BHs terminate with zero entropy on top of the perturbative boson star (black curve).

It is natural to expect that the hairy BHs we find should be the endpoint of the RN instability if we perturb an RN BH in the unstable region (where they always coexist with hairy BHs) and do a time evolution at constant charge and mass. The system would evolve to a final configuration that is stable against the original perturbation while respecting the second law of thermodynamics. Finally note that the hairy BHs with $e_c \leq e < e_{\rm S}$ described in this section were not studied in the perturbative analysis of [26] because the latter can only capture solutions that have a zero mass and charge limit.
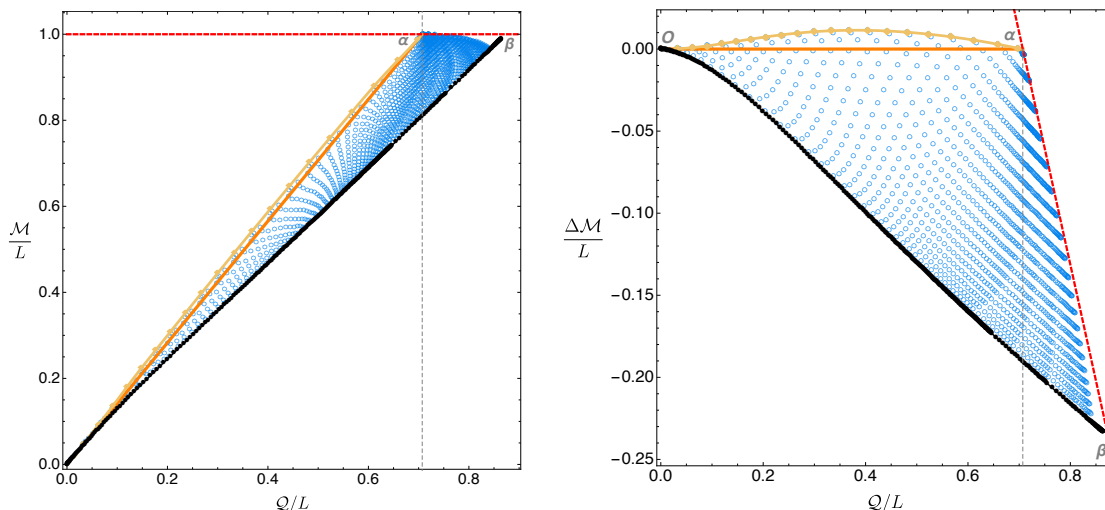
Figure 10. Phase diagram for Einstein theory with a scalar field charge $e = 2.3$ ($e > e_{\rm S}$) in a Minkowski box. In the left panel we have the $\mathcal{Q}$-$\mathcal{M}$ phase diagram: we see that the solutions pile up and this is why we have instead been plotting the phase diagram $\mathcal{Q}$-$\Delta\mathcal{M}$ (right panel). The blue circles describe hairy black holes, the black disk curve is the perturbative soliton family and the orange line is the extremal RN BH (RN black holes exist above it). The yellow curve is the superradiant onset curve of RN. As it could not be otherwise, it agrees with the hairy solutions in the limit where these have $\epsilon = 0$ and thus merge with RN family. The gray and red dashed curves have the same interpretation as in figure 4. For $e > e_{\rm S}$, the zero entropy limit of the hairy BH is the soliton (black disk curve) in the sense that they have the same $(\mathcal{Q}, \mathcal{M})/L$ as the soliton.

4.4 Phase diagram for $e \geq e_{\rm S}$

The critical charge $e = e_{\rm S} = \frac{\pi}{\sqrt{2}} \sim 2.221$ is special for two main (related) reasons. First, it is the minimal charge above which scalar fields can drive *arbitrarily small* extremal RN BHs unstable via superradiance, as observed in the instability onset charge plot of the left panel of figure 1. Indeed, the extremal onset curve $e_{\rm onset}(R_+)$ reaches $e = e_{\rm S}$ as $R_+ \to 0$. The value of $e_{\rm S}$ can be predicted analytically as done in section III.A of [26]. For $e > e_{\rm S}$, we can also have near-extremal BHs unstable for arbitrarily small R_+ or, equivalently, for arbitrarily small mass and charge.

This scalar charge $e_{\rm S}$ is also special because at $e = e_{\rm S}$ the slope of the perturbative soliton at the origin vanishes, *i.e.* $\frac{\delta \Delta\mathcal{M}}{\delta \mathcal{Q}}\big|_{\mathcal{Q}=0} = 0$. For $e < e_{\rm S}$, this slope is positive and we always have (some) perturbative solitons with higher quasilocal mass than the extremal RN (for sufficiently small $\mathcal{Q}$). On the other hand, for $e > e_{\rm S}$ the slope is always negative, $\frac{\delta \Delta\mathcal{M}}{\delta \mathcal{Q}}\big|_{\mathcal{Q}=0} < 0$, and thus perturbative solitons never coexist with RN BHs.

Ultimately as a consequence of these two properties, two important changes occur in the phase diagram of figure 7 as we follow its evolution across $e_{\rm S}$ and land on figure 10. First, the minimal charge for instability — that we have been denoting as $\mathcal{Q}_P$ — approaches zero as $e \to e_{\rm S}^-$ and $\mathcal{Q}_P = 0$ for $e \geq e_{\rm S}$. This is illustrated in figure 10 for the case $e = 2.3$. Second, we find that the hairy BHs (blue circles inside $O\alpha\beta$) now *always* terminate on top of the perturbative boson star (black line $O\beta$) as we move down, *e.g.* at constant $\mathcal{Q}$, from
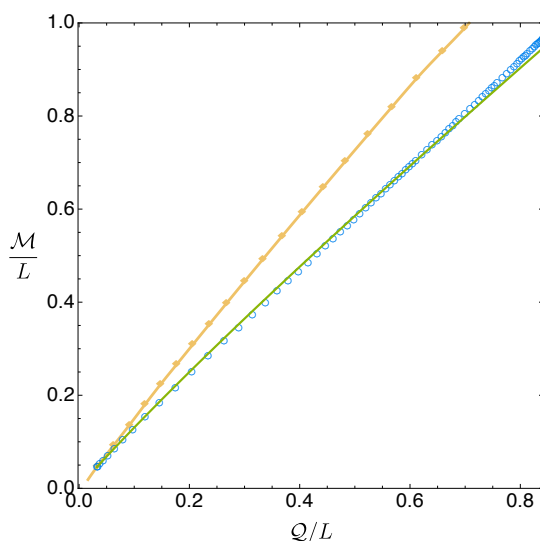
Figure 11. Comparing the exact numerical results (blue circles) with the perturbative analytical predictions (4.2)–(4.3) (green curve) for a family of black holes with constant $R_+ = 0.05$ and $e = 2.3$. As expected, the perturbative analysis matches the exact results only for small R_+ and small ϵ (*i.e.* close to the origin and in the neighbourhood of the merger, yellow diamond, line which has $\epsilon = 0$). That is to say, for the $R_+ = 0.05$ family shown, good agreement occurs for small $\mathcal{Q}$, say $\mathcal{Q} \lesssim 0.2$.

the onset curve $O\alpha$. That is to say, one also has $\mathcal{Q}_\star = 0$ for $e \geq e_{\rm s}$. As hairy BHs approach this perturbative soliton curve, the Kretschmann curvature at the horizon, the entropy and temperature have the same behaviour as the one observed in figure 4 for BHs terminating along $\star\beta$: $K|_{\mathcal{H}} \to \infty$, $S \to 0$ and $T \to \infty$.

Since for $e \geq e_{\rm s}$ the hairy BHs exist all the way down to $(\mathcal{Q}, \mathcal{M}) \to (0,0)$ one might expect that their properties can be captured by a perturbative analysis (to higher orders) around Minkowski space with gauge field in a box. This is indeed the case and such analysis was performed in [26]. This is a double expansion perturbation theory with the expansion parameters being the horizon radius R_+ and the scalar amplitude ϵ. Of course, here one assumes that $R_+ \ll 1$ and $\epsilon \ll 1$ which translates into $\mathcal{Q} \ll 1$ and $\mathcal{M} \ll 1$. The analysis of [26] culminates with explicit expansions for the thermodynamic quantities of the hairy BHs, which are listed in (5.27) of [26]. In particular, the expansion for the quasilocal mass and charge are:

$$
\begin{aligned}
\mathcal{M}/L = &\left[\frac{R_+}{4} \left(\frac{\pi^2}{e^2} + 2 \right) + \frac{R_+^2}{32 e^4} \left(\pi^4 \Big(8[\mathrm{Ci}(2\pi) - \gamma - \ln(2\pi)] + 5 \Big) \right. \right. \\
&\left. \left. \hspace{5cm} + 4 \left(e^2 + \pi^2 \right) e^2 \right) + \mathcal{O}(R_+^3) \right] \\
&+ \epsilon^2 \left[\frac{1}{2} + \frac{R_+}{12\pi e^2} \left(9\pi^3 \Big[\gamma - \mathrm{Ci}(2\pi) - 2 + \ln(2\pi) \Big] \right. \right. \\
&\left. \left. \hspace{4cm} + \left(8\pi^2 - 3e^2 \right) \Big[2\mathrm{Si}(2\pi) - \mathrm{Si}(4\pi) \Big] \right) + \mathcal{O}(R_+^2) \right] \\
&+ \epsilon^4 \left[\frac{15\pi^2 - 6e^2 + 16\pi \big[\mathrm{Si}(4\pi) - 2\mathrm{Si}(2\pi) \big]}{24\pi^2} + \mathcal{O}(R_+) \right] + \mathcal{O}(\epsilon^6),
\end{aligned}
\tag{4.2}
$$

$$\mathcal{Q}/L = \left[\frac{\pi R_+}{2e} + \frac{R_+^2}{8e^3} \Big(\pi^3 \big(2[\mathrm{Ci}(2\pi) - \gamma - \ln(2\pi)] + 1 \big) + 2\pi e^2 \Big) + \mathcal{O}(R_+^3) \right]$$
$$+ \epsilon^2 \left[\frac{e}{2\pi} + \frac{R_+}{12\pi^2 e} \Big(12\pi^3 \Big(\gamma - \mathrm{Ci}(2\pi) + \ln(2\pi) - \frac{7}{4} \Big) \right.$$
$$\left. + \big(8\pi^2 - 3e^2 \big) \left[2\mathrm{Si}(2\pi) - \mathrm{Si}(4\pi) \right] \Big) + \mathcal{O}(R_+^2) \right]$$
$$- \epsilon^4 \left[\frac{e \left(\left(8\pi^2 - e^2 \right) \left(2\mathrm{Si}(2\pi) - \mathrm{Si}(4\pi) \right) + 4\pi e^2 - 8\pi^3 \right)}{8\pi^4} + \mathcal{O}(R_+) \right] + \mathcal{O}(\epsilon^6), \quad (4.3)$$

where $\mathrm{Ci}(x) = - \int_x^\infty \frac{\cos z}{z} \mathrm{d}z$ and $\mathrm{Si}(x) = \int_0^x \frac{\sin z}{z} \mathrm{d}z$ are the cosine and sine integral functions, respectively, and $\gamma \sim 0.577216$ is Euler's constant. This perturbation scheme assumes that R_+ and ϵ do not have a hierarchy of scales. When $R_+ = 0$, (4.2)–(4.3) reduces to the soliton thermodynamics and, when $\epsilon = 0$, (4.2)–(4.3) yields the expansion of the caged RN BH thermodynamics. In [26] it was argued that (4.2)–(4.3) should provide a good approximation (as monitored by the first law) for $\epsilon \lesssim 0.1, R_+ \lesssim 0.1$. Now that we have the exact (numerical) results for the hairy BHs in all their domain of existence we can use (4.2)–(4.3) to further check our numerics while, simultaneously, testing the regime of validity of (4.2)–(4.3). As an example of this exercise, in figure 11 we compare the perturbative prediction (4.2)–(4.3) — the green curve — to our exact numerical results (blue circles) for the 1-parameter family of hairy BHs with $R_+ = 0.05$ parametrized by ϵ (with $\epsilon = 0$ at the merger with RN; the yellow curve). As expected, we observe good agreement for $\mathcal{Q} \lesssim 0.2$, say. Of course, the fact that the perturbative analysis does not differ much from the exact results for higher values of $\mathcal{Q}$ is to be seen as accidental; the perturbative is certainly not valid for such high charges.

As in the previous cases, we end our discussion of the $e \geq e_{\mathrm{s}}$ case with the plot of figure 12 of the entropy as a function of the charge and mass. The colour coding is the same as in previous cases so it suffices to emphasize that again the hairy BHs (blue circles) are the preferred phase in the microcanonical ensemble. Indeed, in the region between the onset yellow curve and the extremal RN dark red curve with $\Delta\mathcal{M} = 0$ where they coexist with (unstable) RN BHs, hairy BHs always have higher dimensionless entropy for a given charge $\mathcal{Q}/L$ and mass $\mathcal{M}/L$. It further follows from the second law, that the unstable RN BHs should evolve in time towards the hairy BH we find with the same $\mathcal{Q}/L$ and $\mathcal{M}/L$.

5 Conclusions and discussion

Recapping what we did so far, we integrated the equations of motion in the domain $R \in [R_+, 1]$ subject to regular boundary conditions at horizon and vanishing scalar field at the box. This is all we need to get the quasilocal phase diagrams of the previous section. But the description of the solution is only complete once we give the full solution all the way up to the asymptotically flat boundary.

Studies of scalar fields confined in a Minkowski cavity are already available in the literature: 1) at the linear level [50–60], 2) within a higher order perturbative analysis of the elliptic problem [21, 26], 3) as a nonlinear elliptic problem (without having asymptotically flat boundary conditions [61–63] or without matching with the exterior solution [64]), and
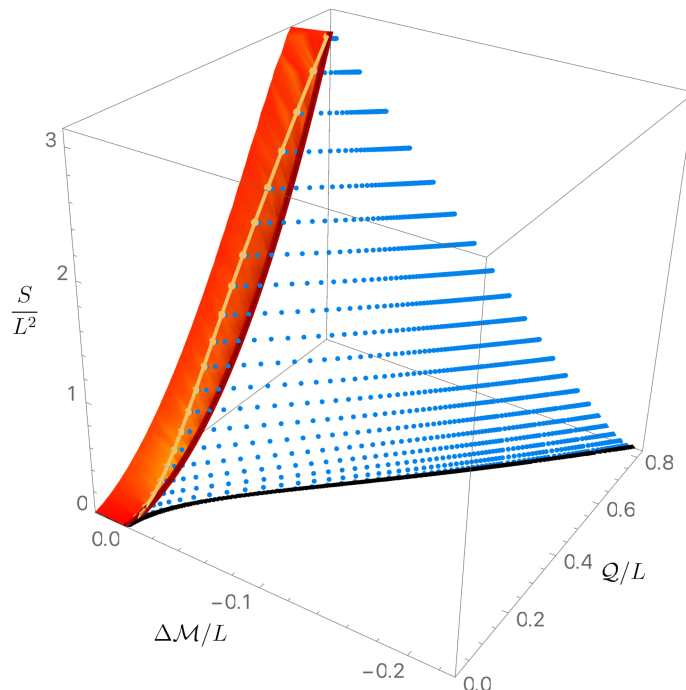
Figure 12. Entropy as a function of the quasilocal charge and mass difference for Einstein theory with a scalar field charge $e = 2.3$ ($e > e_{\rm S}$) in a Minkowski box. When they coexist with RN BHs, for a given $(\mathcal{Q}, \mathcal{M})/L$, hairy BHs always have more entropy than RN, *i.e.* they dominate the microcanonical ensemble. For $e > e_{\rm S}$, the zero entropy limit of the hairy BH is the soliton (black disk curve) in the sense that they have the same $(\mathcal{Q}, \mathcal{M})/L$ as the soliton (the temperature and horizon curvature diverges).

4) as an initial-value problem [45–47]. However, with the exception of the perturbative analysis of [26], the properties of the "internal structure" of the cavity required to confine the scalar field and its contribution to the ADM mass and charge that ultimately describe, by Birkhoff's theorem, the exterior RN solution are not discussed.

However, having the interior solution, we can compute the Lanczos-Darmois-Israel surface stress tensor (3.15) that describes the energy-momentum of the box Σ. We impose the three Israel junction conditions (3.14a)–(3.14c) on the gravitoelectric fields on the surface layer Σ. The fields f, A_t, ϕ are then continuous across Σ and the component of the electric field orthogonal to Σ is also C^0 across Σ. The latter means that we can confine the charged scalar condensate without needing to have a surface electric charge density on Σ. The three conditions (3.14a)–(3.14c) permit us to match the interior and exterior solutions, *i.e.* they fix the parameters M_0, c_A, ρ in (3.5) as a function of the reparametrization freedom parameter N introduced in (3.13):

$$ M_0 = \frac{1}{N^2}\left(1 - \frac{A'_t(1)^2}{2}\right) - 1, \qquad c_A = \frac{A'_t(1) + A_1(1)}{N}, \qquad \rho = -\frac{A'_t(1)}{N}. \qquad (5.1) $$

Effectively, these conditions fix the exterior RN solution as a function of the interior solution and of the box's energy-momentum. Not surprisingly, we have a 1-parameter freedom (N)

to choose the box content that is able to confine the scalar condensate. Several cavities can do the job.

Ideally, we would fix N requiring that the gravitational field is not only C^0 but also differentiable across the box. That is, the fourth junction condition (3.14d) would also be obeyed and thus the extrinsic curvature

$$K^t_{\ t} = -\frac{f'(R)}{2f(R)\sqrt{g(R)}}, \qquad K^i_{\ j} = \frac{1}{R\sqrt{g}}\delta^i_{\ j}, \quad (i,j) = (\theta, \varphi), \qquad (5.2)$$

would also be continuous across the box. But, except when $\phi(R) = 0$, no choice of N allows us to simultaneously set $[K^t_t] = 0$ and $[K^i_i] = 0$. All we can do is to fix N requiring that $[K^t_t] = 0$ (at the expense of having $[K^i_i] \neq 0$) or vice-versa, or any other combination.

A choice of N fixes the energy density and pressure of the box since its stress tensor can be written in the perfect fluid form, $\mathcal{S}_{(a)(b)} = \mathcal{E}u_{(a)}u_{(b)} + \mathcal{P}(h_{(a)(b)} + u_{(a)}u_{(b)})$, with $u = f^{-1/2}\partial_t$ and local energy density $\mathcal{E}$ and pressure $\mathcal{P}$ given by

$$\mathcal{E} = -S^t_{\ t}, \qquad \mathcal{P} = S^x_{\ x} = S^\phi_{\ \phi}. \qquad (5.3)$$

We are further constrained to make a choice such that relevant energy conditions are obeyed. Ultimately, failing these would mean that we cannot build the necessary box with the available materials. Different versions of these energy conditions read ($i = \theta, \varphi$) [18]:

$$\text{Weak energy condition:} \quad \mathcal{E} \geq 0 \quad \wedge \quad \mathcal{E} + \mathcal{P}_i \geq 0; \qquad (5.4)$$

$$\text{Strong energy condition:} \quad \mathcal{E} + \mathcal{P}_i \geq 0 \quad \wedge \quad \mathcal{E} + \sum_{i=1}^{2}\mathcal{P}_i \geq 0; \qquad (5.5)$$

$$\text{Null energy condition:} \quad \mathcal{E} + \mathcal{P}_i \geq 0; \qquad (5.6)$$

$$\text{Dominant energy condition:} \quad \mathcal{E} + |\mathcal{P}_i| \geq 0. \qquad (5.7)$$

We have experimented with different choices of N and found that are many selections that indeed satisfy (5.4) (and equally many others that don't). An example of this exercise is given in [28] for the boson star case. Given that there seems to be no preferred choice, we do not do a further aleatory illustration here. Instead, we approach the problem from an experimental perspective. That is to say, in practice, we are given a cavity (that obeys the energy conditions or else it could not have been built with available materials). In principle, we can identify its stress tensor and hence compute N. We then insert this into the Israel matching conditions (5.1) to find the exact RN exterior solution and, in particular, the asymptotic ADM charges. We end up with an asymptotically flat static black hole solution (or boson star [28]) that is regular everywhere except across the box (where the extrinsic curvature has a discontinuity) and that describes confined scalar radiation floating above the horizon and in thermodynamic equilibrium with it. That is to say, we have established that the configuration originally envisioned (in the rotating case) by Zel'dovich [1], Press-Teukolsky [2] and [30–35] using linear considerations indeed exists as a non-linear equilibrium solution of the Einstein-Maxwell-scalar equations. And we further established

that this is the thermal phase that dominates the microcanonical ensemble. In an ongoing programme, we are extending the current analysis to the rotating BH bomb system.

The hairy BHs we find are stable to the RN instabilities (since they merge with RN precisely at the onset of the original instability; see also [61, 62]) and have higher entropy than the RN BHs. It follows from this and the second law of thermodynamics that the charged black hole bomb does not need to break apart: in a time evolution at fixed energy and charge, the unstable RN BH should simply evolve towards the hairy BH we find. It would be interesting to confirm this doing time evolutions along the lines of those performed in [45–47] in the precise setup we described.

Not less interestingly, Minkowski space in a box (no horizon) with a scalar perturbation is itself non-linearly unstable to the formation of a BH for arbitrarily small amplitude [65], very much alike the pure global AdS spacetime [8, 66–72]. The weakly turbulent phenomenon is responsible for this instability [66–70, 73–75]. It would be interesting to study this non-linear instability when the scalar field is charged. Unlike the neutral case, for certain windows of charge and energy, there are now two possible families of BHs and not just the RN one. Therefore a time evolution of the non-linear instability along the lines of [8, 65, 68, 71, 72, 76–79] should lead in some cases to gravitational collapse into an RN BH and in others into a hairy BH (there should also be a wide class of initial data for which no BH should form at all). Accordingly, the evolution details should differ in these different cases.

Acknowledgments

References

[1] Y.B. Zel'dovich, *Generation of waves by a rotating body*, *JETP Lett.* **14** (1971) 180.

[2] W.H. Press and S.A. Teukolsky, *Floating orbits, superradiant scattering and the black-hole bomb*, *Nature* **238** (1972) 211 [INSPIRE].

[3] V. Cardoso, O.J.C. Dias, J.P.S. Lemos and S. Yoshida, *The black hole bomb and superradiant instabilities*, *Phys. Rev. D* **70** (2004) 044039 [*Erratum ibid.* **70** (2004) 049903] [hep-th/0404096] [INSPIRE].

[4] R. Penrose, *Gravitational collapse: the role of general relativity*, *Riv. Nuovo Cim.* **1** (1969) 252.

[5] D. Christodoulou, *Reversible and irreversible transforations in black hole physics*, [*Phys. Rev. Lett.* **25** (1970) 1596](https://...) [INSPIRE].

[6] O.J.C. Dias, G.T. Horowitz and J.E. Santos, *Black holes with only one Killing field*, [*JHEP* **07** (2011) 115](https://...) [[arXiv:1105.4167](https://arxiv.org/abs/1105.4167)] [INSPIRE].

[7] O.J.C. Dias, J.E. Santos and B. Way, *Black holes with a single Killing vector field: black resonators*, [*JHEP* **12** (2015) 171](https://...) [[arXiv:1505.04793](https://arxiv.org/abs/1505.04793)] [INSPIRE].

[8] M.W. Choptuik, O.J.C. Dias, J.E. Santos and B. Way, *Collapse and nonlinear instability of AdS space with angular momentum*, [*Phys. Rev. Lett.* **119** (2017) 191104](https://...) [[arXiv:1706.06101](https://arxiv.org/abs/1706.06101)] [INSPIRE].

[9] T. Ishii and K. Murata, *Black resonators and geons in AdS$_5$*, [*Class. Quant. Grav.* **36** (2019) 125011](https://...) [[arXiv:1810.11089](https://arxiv.org/abs/1810.11089)] [INSPIRE].

[10] T. Ishii, K. Murata, J.E. Santos and B. Way, *Superradiant instability of black resonators and geons*, [*JHEP* **07** (2020) 206](https://...) [[arXiv:2005.01201](https://arxiv.org/abs/2005.01201)] [INSPIRE].

[11] T. Ishii, K. Murata, J.E. Santos and B. Way, *Multioscillating black holes*, [*JHEP* **05** (2021) 011](https://...) [[arXiv:2101.06325](https://arxiv.org/abs/2101.06325)] [INSPIRE].

[12] C.A.R. Herdeiro and E. Radu, *Kerr black holes with scalar hair*, [*Phys. Rev. Lett.* **112** (2014) 221101](https://...) [[arXiv:1403.2757](https://arxiv.org/abs/1403.2757)] [INSPIRE].

[13] G. Denardo and R. Ruffini, *On the energetics of Reissner Nordström geometries*, [*Phys. Lett. B* **45** (1973) 259](https://...) [INSPIRE].

[14] W. Israel, *Singular hypersurfaces and thin shells in general relativity*, [*Nuovo Cim. B* **44S10** (1966) 1](https://...) [*Erratum ibid.* **48** (1967) 463] [INSPIRE].

[15] W. Israel, *Discontinuities in spherically symmetric gravitational fields and shells of radiation*, [*Proc. Royal Soc. London A* **248** (1958) 404](https://...).

[16] K. Kuchar, *Charged shells in general relativity and their gravitational collapse*, *Czech. J. Phys. B* **B18** (1968) 435.

[17] C. Barrabes and W. Israel, *Thin shells in general relativity and cosmology: The Lightlike limit*, [*Phys. Rev. D* **43** (1991) 1129](https://...) [INSPIRE].

[18] R.M. Wald, *General relativity*, Chicago University Press, Chicago U.S.A (1984).

[19] D. Wiltshire, *Spherically symmetric solutions of Einstein-Maxwell theory with a gauss-bonnet term*, [*Phys. Lett. B* **169** (1986) 36](https://...).

[20] R. D'Inverno, *Introducing Einstein's relativity*, Clarendon Press, U.K. (1992).

[21] O.J.C. Dias and R. Masachs, *Charged black hole bombs in a Minkowski cavity*, [*Class. Quant. Grav.* **35** (2018) 184001](https://...) [[arXiv:1801.10176](https://arxiv.org/abs/1801.10176)] [INSPIRE].

[22] P. Breitenlohner and D.Z. Freedman, *Stability in gauged extended supergravity*, [*Annals Phys.* **144** (1982) 249](https://...) [INSPIRE].

[23] S.S. Gubser, *Breaking an Abelian gauge symmetry near a black hole horizon*, [*Phys. Rev. D* **78** (2008) 065034](https://...) [[arXiv:0801.2977](https://arxiv.org/abs/0801.2977)] [INSPIRE].

[24] O.J.C. Dias, R. Monteiro, H.S. Reall and J.E. Santos, *A scalar field condensation instability of rotating Anti-de Sitter black holes*, [*JHEP* **11** (2010) 036](https://...) [[arXiv:1007.3745](https://arxiv.org/abs/1007.3745)] [INSPIRE].

[25] O.J.C. Dias, P. Figueras, S. Minwalla, P. Mitra, R. Monteiro and J.E. Santos, *Hairy black holes and solitons in global AdS$_5$*, [*JHEP* **08** (2012) 117](https://...) [[arXiv:1112.4447](https://arxiv.org/abs/1112.4447)] [INSPIRE].

[26] O.J.C. Dias and R. Masachs, *Evading no-hair theorems: hairy black holes in a Minkowski box*, [*Phys. Rev. D* **97** (2018) 124030](https://...) [[arXiv:1802.01603](https://arxiv.org/abs/1802.01603)] [INSPIRE].

[27] S.L. Liebling and C. Palenzuela, *Dynamical boson stars*, *Living Rev. Rel.* **15** (2012) 6 [arXiv:1202.5809] [INSPIRE].

[28] O.J.C. Dias, R. Masachs and P. Rodgers, *Boson stars and solitons confined in a Minkowski box*, *JHEP* **04** (2021) 236 [arXiv:2101.01203] [INSPIRE].

[29] J.D. Brown and J.W. York, Jr., *Quasilocal energy and conserved charges derived from the gravitational action*, *Phys. Rev. D* **47** (1993) 1407 [gr-qc/9209012] [INSPIRE].

[30] S.W. Hawking, *Black holes and thermodynamics*, *Phys. Rev. D* **13** (1976) 191 [INSPIRE].

[31] G.W. Gibbons and M.J. Perry, *Black holes and thermal Green's functions*, *Proc. Roy. Soc. London A* **358** (1978) 467.

[32] R. Penrose, *Singularities and time-asymmetry*, in *General relativity: an Einstein centenary survey*, S.W. Hawking and W. Israel eds., Cambridge UNiversity Press, Cambridge U.K. (1979).

[33] D.N. Page, *Black hole formation in a box*, *Gen. Rel. Grav.* **13** (1981) 1117 [INSPIRE].

[34] S.W. Hawking and D.N. Page, *Thermodynamics of black holes in Anti-de Sitter space*, *Commun. Math. Phys.* **87** (1983) 577 [INSPIRE].

[35] H.W. Braden, J.D. Brown, B.F. Whiting and J.W. York, Jr., *Charged black hole in a grand canonical ensemble*, *Phys. Rev. D* **42** (1990) 3376 [INSPIRE].

[36] T. Andrade, W.R. Kelly, D. Marolf and J.E. Santos, *On the stability of gravity with Dirichlet walls*, *Class. Quant. Grav.* **32** (2015) 235006 [arXiv:1504.07580] [INSPIRE].

[37] P. Basu, J. Bhattacharya, S. Bhattacharyya, R. Loganayagam, S. Minwalla and V. Umesh, *Small hairy black holes in global AdS spacetime*, *JHEP* **10** (2010) 045 [arXiv:1003.3232] [INSPIRE].

[38] S. Bhattacharyya, S. Minwalla and K. Papadodimas, *Small hairy black holes in* $AdS_5 \times S^5$, *JHEP* **11** (2011) 035 [arXiv:1005.1287] [INSPIRE].

[39] S.A. Gentle, M. Rangamani and B. Withers, *A soliton menagerie in AdS*, *JHEP* **05** (2012) 106 [arXiv:1112.3979] [INSPIRE].

[40] R. Arias, J. Mas and A. Serantes, *Stability of charged global AdS₄ spacetimes*, *JHEP* **09** (2016) 024 [arXiv:1606.00830] [INSPIRE].

[41] J. Markeviciute and J.E. Santos, *Hairy black holes in* $AdS_5 \times S^5$, *JHEP* **06** (2016) 096 [arXiv:1602.03893] [INSPIRE].

[42] J. Markeviciute, *Rotating Hairy Black Holes in* $AdS_5 \times S^5$, *JHEP* **03** (2019) 110 [arXiv:1809.04084] [INSPIRE].

[43] O.J.C. Dias and R. Masachs, *Hairy black holes and the endpoint of AdS₄ charged superradiance*, *JHEP* **02** (2017) 128 [arXiv:1610.03496] [INSPIRE].

[44] R.L. Arnowitt, S. Deser and C.W. Misner, *The dynamics of general relativity*, *Gen. Rel. Grav.* **40** (2008) 1997 [gr-qc/0405109].

[45] N. Sanchis-Gual, J.C. Degollado, P.J. Montero, J.A. Font and C. Herdeiro, *Explosion and final state of an unstable Reissner-Nordström black hole*, *Phys. Rev. Lett.* **116** (2016) 141101 [arXiv:1512.05358] [INSPIRE].

[46] N. Sanchis-Gual, J.C. Degollado, C. Herdeiro, J.A. Font and P.J. Montero, *Dynamical formation of a Reissner-Nordström black hole with scalar hair in a cavity*, *Phys. Rev. D* **94** (2016) 044061 [arXiv:1607.06304] [INSPIRE].

[47] N. Sanchis-Gual, J.C. Degollado, J.A. Font, C. Herdeiro and E. Radu, *Dynamical formation of a hairy black hole in a cavity from the decay of unstable solitons*, *Class. Quant. Grav.* **34** (2017) 165001 [arXiv:1611.02441] [INSPIRE].

[48] C.W. Misner, K.S. Thorne and J.A. Wheeler, *Gravitation*, W.H. Freeman and Co., San Francisco U.S.A. (1973).

[49] O.J.C. Dias, J.E. Santos and B. Way, *Numerical methods for finding stationary gravitational solutions*, *Class. Quant. Grav.* **33** (2016) 133001 [arXiv:1510.02804] [INSPIRE].

[50] C.A.R. Herdeiro, J.C. Degollado and H.F. Rúnarsson, *Rapid growth of superradiant instabilities for charged black holes in a cavity*, *Phys. Rev. D* **88** (2013) 063003 [arXiv:1305.5513] [INSPIRE].

[51] S. Hod, *Analytic treatment of the charged black-hole-mirror bomb in the highly explosive regime*, *Phys. Rev. D* **88** (2013) 064055 [arXiv:1310.6101] [INSPIRE].

[52] J.C. Degollado and C.A.R. Herdeiro, *Time evolution of superradiant instabilities for charged black holes in a cavity*, *Phys. Rev. D* **89** (2014) 063005 [arXiv:1312.4579] [INSPIRE].

[53] S. Hod, *Resonance spectra of caged black holes*, *Eur. Phys. J. C* **74** (2014) 3137 [arXiv:1410.4567] [INSPIRE].

[54] R. Li, J.-K. Zhao and Y.-M. Zhang, *Superradiant instability of D-dimensional Reissner-Nordström black hole mirror system*, *Commun. Theor. Phys.* **63** (2015) 569 [arXiv:1404.6309] [INSPIRE].

[55] S. Hod, *The charged black-hole bomb: a lower bound on the charge-to-mass ratio of the explosive scalar field*, *Phys. Lett. B* **755** (2016) 177 [arXiv:1606.00444] [INSPIRE].

[56] O. Fierro, N. Grandi and J. Oliva, *Superradiance of charged black holes in Einstein-Gauss-Bonnet gravity*, *Class. Quant. Grav.* **35** (2018) 105007 [arXiv:1708.06037] [INSPIRE].

[57] R. Li and J. Zhao, *Superradiant instability of charged scalar field in stringy black hole mirror system*, *Eur. Phys. J. C* **74** (2014) 3051 [arXiv:1403.7279] [INSPIRE].

[58] R. Li and J. Zhao, *Numerical study of superradiant instability for charged stringy black hole-mirror system*, *Phys. Lett. B* **740** (2015) 317 [arXiv:1412.1527] [INSPIRE].

[59] R. Li, Y. Tian, H.-b. Zhang and J. Zhao, *Time domain analysis of superradiant instability for the charged stringy black hole-mirror system*, *Phys. Lett. B* **750** (2015) 520 [arXiv:1506.04267] [INSPIRE].

[60] R. Li, J. Zhao, X. Wu and Y. Zhang, *Scalar clouds in charged stringy black hole-mirror system*, *Eur. Phys. J. C* **75** (2015) 142 [arXiv:1501.07358] [INSPIRE].

[61] S.R. Dolan, S. Ponglertsakul and E. Winstanley, *Stability of black holes in Einstein-charged scalar field theory in a cavity*, *Phys. Rev. D* **92** (2015) 124047 [arXiv:1507.02156] [INSPIRE].

[62] S. Ponglertsakul, E. Winstanley and S.R. Dolan, *Stability of gravitating charged-scalar solitons in a cavity*, *Phys. Rev. D* **94** (2016) 024031 [arXiv:1604.01132] [INSPIRE].

[63] S. Ponglertsakul and E. Winstanley, *Effect of scalar field mass on gravitating charged scalar solitons and black holes in a cavity*, *Phys. Lett. B* **764** (2017) 87 [arXiv:1610.00135] [INSPIRE].

[64] P. Basu, C. Krishnan and P.N. Bala Subramanian, *Hairy black holes in a box*, *JHEP* **11** (2016) 041 [arXiv:1609.01208] [INSPIRE].

[65] M. Maliborski and A. Rostworowski, *Time-periodic solutions in an Einstein AdS-massless-scalar-field system*, *Phys. Rev. Lett.* **111** (2013) 051102 [arXiv:1303.3186] [inSPIRE].

[66] M. Dafermos, *The black hole stability problem*, talk given at the Newton Institute, University of Cambridge, Cambridge U.K. (2006), http://www-old.newton.ac.uk/webseminars/pg+ws/2006/gmx/1010/dafermos/,

[67] M. Dafermos and G. Holzegel, *Dynamic instability of solitons in* $4 + 1$ *dimensional gravity with negative cosmological constant*, seminar at DAMTP, University of Cambridge, Cambridge U.K. (2006), https://www.dpmms.cam.ac.uk/~md384/ADSinstability.pdf.

[68] P. Bizon and A. Rostworowski, *On weakly turbulent instability of Anti-de Sitter space*, *Phys. Rev. Lett.* **107** (2011) 031102 [arXiv:1104.3702] [inSPIRE].

[69] O.J.C. Dias, G.T. Horowitz and J.E. Santos, *Gravitational turbulent instability of Anti-de Sitter space*, *Class. Quant. Grav.* **29** (2012) 194002 [arXiv:1109.1825] [inSPIRE].

[70] O.J.C. Dias, G.T. Horowitz, D. Marolf and J.E. Santos, *On the nonlinear stability of asymptotically Anti-de Sitter solutions*, *Class. Quant. Grav.* **29** (2012) 235019 [arXiv:1208.5772] [inSPIRE].

[71] A. Buchel, L. Lehner and S.L. Liebling, *Scalar collapse in AdS*, *Phys. Rev. D* **86** (2012) 123011 [arXiv:1210.0890] [inSPIRE].

[72] A. Buchel, S.L. Liebling and L. Lehner, *Boson stars in AdS spacetime*, *Phys. Rev. D* **87** (2013) 123006 [arXiv:1304.4166] [inSPIRE].

[73] O. Dias and J.E. Santos, *AdS nonlinear instability: moving beyond spherical symmetry*, *Class. Quant. Grav.* **33** (2016) 23LT01 [arXiv:1602.03890] [inSPIRE].

[74] A. Rostworowski, *Comment on "AdS nonlinear instability: moving beyond spherical symmetry" [Class. Quantum Grav. 33 23LT01 (2016)]*, *Class. Quant. Grav.* **34** (2017) 128001 [arXiv:1612.00042] [inSPIRE].

[75] O.J.C. Dias and J.E. Santos, *AdS nonlinear instability: breaking spherical and axial symmetries*, *Class. Quant. Grav.* **35** (2018) 185006 [arXiv:1705.03065] [inSPIRE].

[76] V. Balasubramanian, A. Buchel, S.R. Green, L. Lehner and S.L. Liebling, *Holographic thermalization, stability of Anti-de Sitter space, and the Fermi-Pasta-Ulam paradox*, *Phys. Rev. Lett.* **113** (2014) 071601 [arXiv:1403.6471] [inSPIRE].

[77] P. Bizoń and A. Rostworowski, *Comment on "Holographic thermalization, stability of Anti-de Sitter space, and the Fermi-Pasta-Ulam Paradox"*, *Phys. Rev. Lett.* **115** (2015) 049101 [arXiv:1410.2631] [inSPIRE].

[78] E. da Silva, E. Lopez, J. Mas and A. Serantes, *Collapse and revival in holographic quenches*, *JHEP* **04** (2015) 038 [arXiv:1412.6002] [inSPIRE].

[79] V. Balasubramanian, A. Buchel, S.R. Green, L. Lehner and S.L. Liebling, *Reply to Comment on "Holographic thermalization, stability of Anti-de Sitter space, and the Fermi-Pasta-Ulam paradox"*, *Phys. Rev. Lett.* **115** (2015) 049102 [arXiv:1506.07907] [inSPIRE].